Atmospheric Environment 340 (2025) 120896

Contents lists available at ScienceDirect

Atmospheric Environment

journal homepage: www.elsevier.com/locate/atmosenv

Investigating uncertainties in air quality models used in GMAP/SIJAQ 2021 field campaign: General performance of different models and ensemble results

Yesol Cha[a,b,1], Jong-Jae Lee[a,c,1], Chul Han Song[d], Soontae Kim[e], Rokjin J. Park[f], Myong-In Lee[a], Jung-Hun Woo[g], Jae-Ho Choi[a], Kangho Bae[a], Jinhyeok Yu[d], Eunhye Kim[i], Hyeonmin Kim[f], Seung-Hee Lee[a], Jinseok Kim[h], Lim-Seok Chang[j], Kwon-ho Jeon[k], Chang-Keun Song[a,b,c,*]

[a] *Department of Civil Urban Earth and Environmental Engineering, Ulsan National Institute of Science and Technology (UNIST), Ulsan, Republic of Korea*
[b] *Graduate School of Carbon Neutrality, Ulsan National Institute of Science and Technology (UNIST), Ulsan, Republic of Korea*
[c] *Research & Management Center for Particulate Matters at the Southeast Region of Korea, Ulsan National Institute of Science and Technology (UNIST), Ulsan 44919, Republic of Korea*
[d] *School of Earth Sciences and Environmental Engineering, Gwangju Institute of Science and Technology (GIST), Gwangju 61005, Republic of Korea*
[e] *Department of Environmental and Safety Engineering, Ajou University, Suwon, Republic of Korea*
[f] *School of Earth and Environmental Sciences, Seoul National University, Seoul, Republic of Korea*
[g] *Graduate School of Environmental Studies, Seoul National University, Seoul, Republic of Korea*
[h] *Department of Advanced Technology Fusion, Konkuk University, Seoul, Republic of Korea*
[i] *Department of Environmental Engineering, Kunsan National University, Kunsan, Republic of Korea*
[j] *Environmental Satellite Center, National Institute of Environmental Research, Incheon 22689, Republic of Korea*
[k] *Department of Climate and Air Quality Research, National Institute of Environmental Research (NIER), Incheon, Republic of Korea*

HIGHLIGHTS

- The model performance in this study improved compared to the KORUS-AQ campaign.
- Inaccurate meteorological inputs, such as precipitation, RH, and PBLH degrade the model performance.
- Uncertainty in the emission inventory can lead to extreme underestimation or overestimation of the CTMs.

ARTICLE INFO

Keywords:
Air quality
GMAP/SIJAQ 2021 field campaign
Model ensemble
Performance evaluation

ABSTRACT

The international field campaign, GMAP/SIJAQ 2021, was conducted in Korea from October 18th to November 25th to enhance the performance and validation of the Geostationary Environment Monitoring Spectrometer (GEMS) products algorithm and obtain a better understanding of the current air pollution status of the Korean Peninsula. Five chemical transport models (CTMs), including CMAQ, CMAQ-GIST, CAMx, WRF-Chem, and WRF GEOS-Chem, were utilized during the campaign to assist in organizing the observation plan and identifying

Abbreviations: CTMs, Chemical transport models; CF, Coarse/fine scheme; CMAQ, Community Multiscale Air Quality Modeling System; CAMx, Comprehensive Air Quality Model with Extensions; EC, Elemental carbon; EBI, Euler Backward Iterative; FNL, Final; GCAS, GeoCAPE Airborne Simulator; GEMS, Geostationary Environment Monitoring Spectrometer; GFS, Global Forecast System; GOCART, Goddard Chemistry Aerosol Radiation and Transport; GIST, Gwangju Institute of Science and Technology; IOA, Index of Agreement; KORUS-AQ, Korea–United States Air Quality; MB, Mean Bias; MEGAN, Model of Emissions of Gases and Aerosols from Nature; MARGA, Monitor for Aerosols and Gases; MAX-DOAS, Multi-axis Differential Optical Absorption Spectrometer; NCEP, National Center for Environmental Prediction; NIER, National Institute of Environmental Research; NMB, Normalized Mean Bias; OM, Organic matter; PBLH, Planetary boundary layer height; RH, Relative humidity; RMSE, Root Mean Square Error; SOA, Secondary organic aerosols; SMA, Seoul Metropolitan Area; VOCs, Volatile Organic Compounds; WRF, Weather Research and Forecasting; WSM5, WRF Single Moment 5-class.

* Corresponding author. Department of Civil Urban Earth and Environmental Engineering, Ulsan National Institute of Science and Technology (UNIST), Ulsan, Republic of Korea.

E-mail address: cksong@unist.ac.kr (C.-K. Song).

[1] Both authors contributed equally as first author.

https://doi.org/10.1016/j.atmosenv.2024.120896
Received 26 March 2024; Received in revised form 15 October 2024; Accepted 25 October 2024
Available online 29 October 2024

changes in pollutant concentrations and their spatiotemporal distribution in Korea following the Korea–United States Air Quality (KORUS-AQ) 2016. In this study, we evaluated the forecasting performance, strengths, and limitations of these five CTMs and their ensemble in simulating air quality. Intensive measurement data and intercomparisons were employed to explain discrepancies between observed and simulated results. A comparison of the CTM ensemble results for $PM_{2.5}$ and various gaseous pollutants between the current GMAP/SIJAQ 2021 and previous KORUS-AQ 2016 campaigns showed the R-value for the total mass $PM_{2.5}$ concentration increased from 0.88 to 0.94. This improvement is related to CTM updates, including the emission inventory and better reproductions of the concentrations of gaseous species. However, the models consistently underestimated carbon monoxide (CO) concentrations, similar to the results from KORUS-AQ. This finding still suggests a further challenge that requires consideration of missing anthropogenic sources. The results of the ensemble model agreed well with the chemical composition of $PM_{2.5}$ observed at the intensive monitoring station. However, for NO_3^- and NH_4^+, discrepancies were primarily due to inaccuracies in the meteorological inputs, such as precipitation, relative humidity (RH), and nighttime planetary boundary layer height (PBLH) in the CTMs. Hence, all models overestimated the concentration of elemental carbon (EC), therefore, it is necessary to revise EC emissions in the SIJAQv2 inventory, as these apply to unusual levels recorded in Seoul during the reference year of 2018.

1. Introduction

Air Pollution is a global concern, and numerous efforts are being made to address this effectively, given its direct impact on human health. The Korean government launched the world's first Geostationary Environment Monitoring Spectrometer (GEMS) satellite, which consistently observes various atmospheric chemical components and their composition over East Asian regions, including the Korean Peninsula. To improve the performance of the GEMS science algorithm, validate its products, and deepen our understanding of the spatial and temporal distributions of air pollutants over the Korean Peninsula, the National Institute of Environmental Research (NIER), Korea, conducted an international intensive field campaign, GMAP (GEMS MAP of Air Pollution)/SIJAQ (Satellite Integrated Joint Monitoring of Air Quality), from October to November 2021.

For this intensive campaign, data were gathered from various ground-based remote sensing instruments. The Multi-axis Differential Optical Absorption Spectrometer (MAX-DOAS) and the Pandora spectrometer were employed in ground-based remote sensing settings. To enhance the coverage of our ground-based remote sensing observation network, additional instruments were introduced. Car-DOAS measurements and flight measurements using the GeoCAPE Airborne Simulator (GCAS) were conducted in the Seoul Metropolitan Area (SMA) and the southeastern region of Korea. Car-DOAS is a remote sensing instrument mounted on a vehicle, and GCAS is deployed on a Cessna aircraft. Both were used to capture the emission source distribution more comprehensively. Information from both geostationary and polar environmental satellites, along with meteorological data, were also utilized.

Numerical simulations were conducted to improve our understanding of the spatiotemporal distribution of particulate matter and gaseous chemical species. In these simulations, five different Chemical Transport Models (CTMs) were employed: the Community Multiscale Air Quality Modeling System (CMAQ), the CMAQ- Gwangju Institute of Science and Technology (GIST), the Comprehensive Air Quality Model with Extensions (CAMx), the Weather Research and Forecasting model coupled with Chemistry (WRF-Chem), and the WRF_GEOS-Chem. These models maintained a spatial resolution of 27 km for East Asia, 9 km for the Korean Peninsula, and 3 km for both the SMA and the Southeast region of South Korea.

The results and ensemble statistics of each model were used to thoroughly analyze the ground-based remote sensing data and prepare a relevant flight path for aircraft measurements during the campaign. When combined with intensive observational data, these comprehensive studies also helped to identify and address the inherent limitations of the models, including various technical and scientific modeling challenges (such as temporal/spatial resolution issues), uncertainties associated with chemical mechanisms, and estimations of emissions. Previous studies have already indicated that an ensemble of multiple models can reduce these uncertainties, often resulting in improved model performance (Chen et al., 2019; Im et al., 2018; Ma et al., 2019; Petersen et al., 2019).

A similar international intensive observation campaign was previously conducted across South Korea in 2016 through a collaboration between the U.S. NASA and the National Institute of Environmental Research of Korea. In this respect, the Korea–United States Air Quality (KORUS-AQ) field study was conducted from May to June 2016. The data collected from this study remain valuable and provide a scientific basis for enhancing our understanding of the factors influencing national air quality regulations and international cooperation efforts (Crawford et al., 2021). During the KORUS-AQ campaign, six regional and two global chemistry transport models were used to elucidate the formation processes of various aerosols, especially secondary organic aerosols (Kim et al., 2018; Nault et al., 2018) and long-range transport phenomena (Choi et al., 2019; Lee et al., 2019). In addition, various observational data and analyses from the campaign were utilized to evaluate the performance of these different models using an inter-comparison approach (Park et al., 2021).

In this study, we aimed to evaluate the forecasting performance of the five different CTMs using intensive measurement data during the campaign period to understand the characteristics of each CTM and identify its strengths and limitations in simulating air quality. An ensemble of multiple models was also examined, and intercomparisons between the five CTMs were made to comprehensively explain discrepancies between observed values and simulated results.

2. Methods

2.1. Model description

Four regional and one global CTMs were employed to perform air quality simulations focusing on $PM_{2.5}$ and O_3 during the GMAP/SIJAQ period. All simulations utilized identical anthropogenic emissions from the GMAP/SIJAQv2 inventory for East Asia, which was based on the emissions inventories developed by Woo et al. (2020).

In this study, the CMAQ (Byun and Schere, 2006) version 5.2 was used to predict gaseous and aerosol air pollutants during the campaign. The mechanism 'cb6r3_ae6_aq' was applied according to the photochemistry Carbon Bond 6 (Yarwood et al., 2010) version and the 6th generation aerosol module for secondary organic aerosols (SOAs). The Euler Backward Iterative (EBI) chemistry solver is employed for the photochemical mechanism. The initial and boundary input fields were generated using the default boundary condition profile provided by the CMAQ model, which represents typical atmospheric conditions at the model's boundaries.

The GIST has developed, and recently updated CMAQ-GIST (hereafter CMAQ_G) based on the CMAQ v5.2 model. Daytime HONO chemistries were revised in this model based on the SAPRC07TC chemical mechanism (Zhang et al., 2016), and yield data for SOA formation for the two-product approach (Odum et al., 1996) was updated using data from multiple smog chamber experiments conducted under typical northeast Asian atmospheric conditions (Babar et al., 2016). To provide boundary conditions, seasonal climatology was obtained from the hemispheric CMAQ model output (Hogrefe et al., 2018). Initial conditions were updated every 15 UTC (i.e., 00 KST) via 3D-Var data assimilation with ground-based observations $PM_{2.5}$ from Korea and China (Lee et al., 2022a,b).

The WRF-Chem is an online, non-hydrostatic, mesoscale air quality model (Grell et al., 2005; Skamarock and Klemp, 2008). In the online mode, the chemical module uses the same transport, physics schemes, and grid as the meteorological module. The gas phase chemistry model is used in Ozone and Related Chemical Tracers version 4 (MOZART-4) (Emmons et al., 2010). The aerosol module includes the Goddard Chemistry Aerosol Radiation and Transport (GOCART) module, which simulates major tropospheric aerosol components, including sulfate, dust, black and organic carbon, and sea salt. It includes algorithms for dust and sea salt emissions, dry deposition, and gravitational settling. The mozbc tool was used to determine the chemical initial and lateral boundary conditions (https://www2.acom.ucar.edu/wrf-chem/wrf-chem-tools-community), using global model results from the Whole Atmosphere Community Climate Model (WACCM), which is driven by meteorological fields from the NASA GMAO GEOS-5 model.

CAMx version 7.1 was used to predict gaseous air pollutants and $PM_{2.5}$. CAMx includes RADM-AQ for inorganic aqueous chemistry, ISORROPIA for inorganic gas-aerosol partitioning, and SOAP for organic gas-aerosol partitioning and oxidation (ENVIRON, 2006). SAPRC07TC with a two-mode coarse/fine scheme (CF) was applied for the chemical mechanism and particle size distribution. WRF and SMOKE were employed to generate meteorological data and emission inputs for CAMx, while the chemical initial and boundary conditions for CAMx were derived from the CMAQ default profile, processed using CMAQ2CAMx.

The WRF_GC is a chemical transport model that integrates the Weather Research and Forecasting (WRF) mesoscale meteorological model and the Goddard Earth Observing System with a chemistry model (GEOS-Chem version 12.1.1) (Feng et al., 2021; Lin et al., 2020). Grid and subgrid-scale clouds were treated based on the WRF Single Moment 5-class (WSM5) (Hong et al., 2004) and the newer Tiedtke scheme (Tiedtke, 1989; Zhang et al., 2011). The chemical boundary conditions were determined every hour using GRIMs-CCM, developed by coupling the chemistry modules of the GEOS-Chem to the GRIMs general circulation model (Koo et al., 2023; Seungun Lee et al., 2022a, 2022b). The tropospheric chemistry (GEOS-Chem Tropchem) of GEOS-Chem was applied for the chemical mechanism.

Each model used in this study had a different simulation domain; therefore, the target area and spatial resolution of each model varied. In this respect, CMAQ, WRF-Chem, and CAMx use a nested simulation (9 km) with an outer domain of 27 km resolution covering East Asia. WRF_GC uses a nested domain with a spatial resolution of 9 km for Korea with boundary conditions determined from a 0.25° x 0.3125° GRIMs-CCM simulation. The CMAQ_G uses 15 x 15 km horizontal resolution over the northeast Asia domain.

Tables 1 and 2 summarize the details of the participating models, including their employed meteorology, a grid resolution of the simulations, biogenic emissions schemes, chemistry mechanisms, and aerosol thermodynamics. We allowed each model to select its own configurations for meteorological fields and natural emissions. As demonstrated in the table, substantial differences were noted between the models in terms of gas-phase chemistry mechanisms and aerosol mechanisms.

2.2. Emissions

The model-ready anthropogenic emissions as CTM input data (GMAP/SIJAQv2) were processed according to the latest national emission inventory, the relevant temporal/spatial allocation, and the appropriate chemical lumping scheme for each model. The inventory included area, mobile, ship, and point emissions of species such as CO, SO_2, NO_X, NH_3, and volatile organic compounds (VOCs). Compared to the existing emissions prepared for KORUS-AQ, the base reference year of the emission dataset was updated to 2017 for China and Japan and 2018 for South Korea. Table 3 and Fig. 1 show the emission inventories by country used in GMAP/SIJAQv2 and the difference between KORUSv5 and GMAP/SIJAQv2.

The most significant change in emissions compared to the KORUSv5 emission inventory was found in China. Specifically, SO_2 emissions decreased by approximately 29.5%, from approximately 13.3 Tg/yr in 2016 to approximately 9.4 Tg/yr in 2017. NH_3 emissions showed a reduction of approximately 2.7%, decreasing from approximately 10.3 Tg/yr in 2016 to approximately 10.1 Tg/yr in 2017. While emissions in Korea showed a notable decrease in SO_X and NO_X, NH_3 emissions

Table 2
Summary of model resolution and PBL scheme of models participating in the intercomparison.

Model	Institution	Horizontal Resolution	Vertical Levels (Model Top Height)	PBL scheme
CMAQ v5.2	UNIST	27 × 27 km (East Asia) 9 × 9 km (Korea)	23 (50 hPa)	YSU
CMAQ-GIST	GIST	15 × 15 km (East Asia)	15 (50 hPa)	YSU
WRF-Chem v3.9.1	UNIST	27 × 27 km (East Asia) 9 × 9 km (Korea)	31 (50 hPa)	YSU
CAMx v7.1	Ajou Univ	27 × 27 km (East Asia) 9 × 9 km (Korea)	15 (50 hPa)	YSU
WRF-GC v12.1.1	Seoul Nat'l Univ (SNU)	9 × 9 km (Korea)	47 (80 km)	YSU

Table 1
Summary of input, chemistry, and aerosol options of models participating in the intercomparison.

Model	Institution	Meteorology	Biogenic Emission	Wildfire Emission	Chemistry Mechanism	Aerosol Thermodynamics + Microphysics
CMAQ v5.2	UNIST	GFS 0.5° FNL 0.25°	MEGAN v2.1	–	CB6r3	ISORROPIA II + AERO6
CMAQ-GIST	GIST	GFS 0.25° FNL 0.25°	MEGAN v2.1	FINN v1.5	Modified SAPRC07TC	ISORROPIA II + AERO6
WRF-Chem v3.9.1	UNIST	GFS 0.5° FNL 0.25°	MEGAN v2.04	–	MOZART	GOCART + Lin Scheme
CAMx v7.1	Ajou Univ	GFS 1.0° FNL 0.25°	MEGAN v2.0	–	SAPRC07	ISORROPIA II + CF scheme
WRF-GC v12.1.1	Seoul Nat'l Univ (SNU)	GFS 0.5° FNL 0.5°	MEGAN v2.1	–	GEOS-Chem Tropchem	ISORROPIA II + Bulk scheme

Table 3
Total anthropogenic emissions (Gg/yr) in the GMAP/SIJAQ version 2 emission inventories of each country.

	CO	NO_X	SO_2	$PM_{2.5}$	VOC	NH_3
S. Korea	763.5	1067.5	291.7	95.3	1020.8	316
China	115,486.2	17,121.9	9434.5	6667.4	23,832.1	10,051.0
Japan	2995.3	1196.3	345.9	53.4	891.9	342.6
Other regions	95,197.4	12,084.8	16,091.3	10,446.9	27,321.9	12,285.3
Total	214,442.3	31,470.6	26,163.4	17,262.9	53,066.8	22,994.8

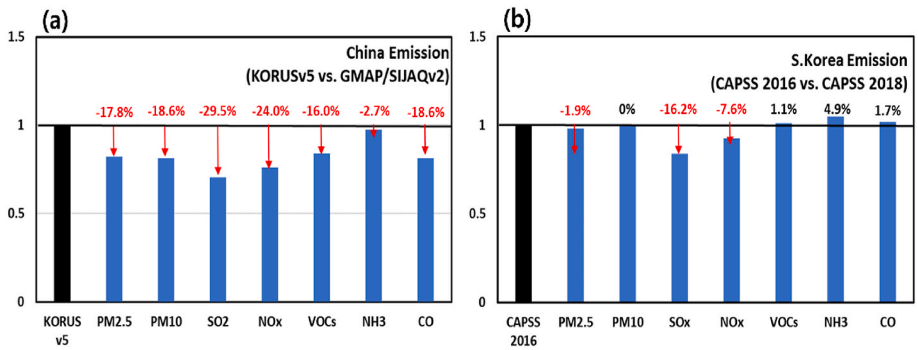

Fig. 1. GMAP/SIJAQv2 emission change rate by material in China (a) and South Korea (b) compared to KORUSv5. (CAPSS; Clean Air Support System in South Korea).

exhibited an increase.

The participating models employed various versions of the Model of Emissions of Gases and Aerosols from Nature (MEGAN), including versions 2.0, 2.04, and 2.1 (Guenther et al., 2012), for biogenic emissions of isoprene, terpenes, and other VOCs. Each model utilized its own vegetation map and meteorology to estimate biogenic emissions, resulting in variations in isoprene emissions among them. Additionally, only CMAQ_G included biomass-burning emissions in its inventory, and emissions from wildfires were generally much lower than those from anthropogenic sources in Korea.

2.3. Observations

The surface mass concentrations obtained from a national-wide urban monitoring network (www.airkorea.or.kr) managed by the National Institute of Environmental Research (NIER) were used to evaluate the performance of five different types of air quality model and determine their ensemble statistics during the GMAP/SIJAQ campaign period. We gathered hourly concentration data for $PM_{2.5}$, O_3, NO_2, SO_2, and CO from 505 Air-Korea monitoring stations. During the GMAP/SIJAQ campaign, chemical components and their precursors were specifically measured using a Monitor for Aerosols and Gases (MARGA) at Olympic Park in Seoul, as depicted in Fig. 2(b). As a result, we obtained hourly concentrations of gaseous pollutants such as O_3, NO_2, SO_2, CO, and NH_3, as well as particulate matter, including NO_3^-, SO_4^{2-}), NH_4^+, organic matter (OM), and elemental carbon (EC).

In addition to surface mass concentrations, we collected various observational data from ground, air, and space using the remote sensing instruments mentioned in the introduction. These efforts aimed to improve our overall understanding of emission patterns and sources. In this study, we evaluated the general performance of the models by focusing only on the ground concentration and chemical composition of $PM_{2.5}$ observed during the campaign period. Research on the vertical distribution and long-range transport phenomena, using remote sensing and satellite data observed during the campaign period, will be conducted as a follow-up to this study.

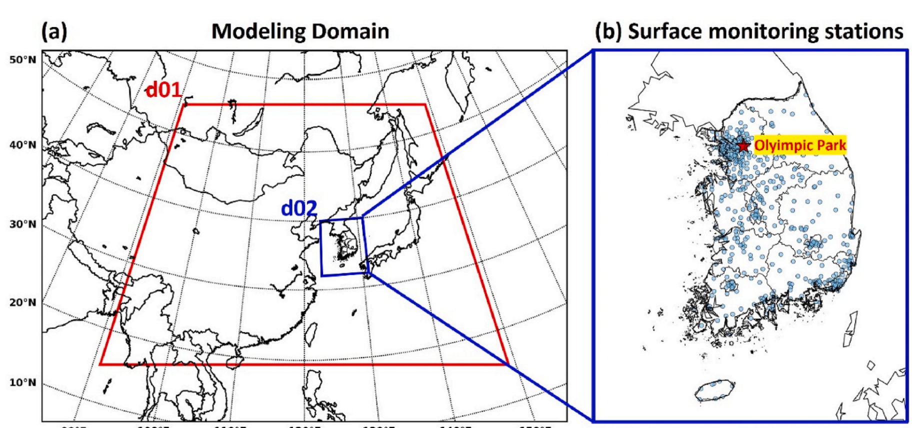

Fig. 2. Ensemble modeling domain for comparing five types of models (CMAQ, CMAQ_G, CAMx, WRF_Chem, and WRF_GC). (a) Domain 1 (d01) with 27 km × 27 km horizontal resolution covering 15–54°N, 91–149°E and domain 2 (d02) with 9 km × 9 km horizontal resolution covering the Korean peninsula, 32–40°N and 123–131°E. (b) The locations of 505 Air-Korea surface monitoring stations (blue) and the intensive monitoring station (red; Olympic Park) during the GMAP campaign are shown.

3. Results

We conducted a performance evaluation of five different models during the GMAP/SIJAQ 2021 campaign by comparing their individual and ensemble results to observed data. This allowed us to assess model biases and understand the causes of discrepancies among the models. For the model evaluation, 9-km resolution results were used, and the CMAQ_G results were interpolated to a 9-km resolution. The hourly model values were then extracted from the grid cells closest to the observation sites to ensure accurate spatial matching. These hourly values were then averaged to daily values, corresponding to the 39-day period from October 18th to November 25th during the GMAP/SIJAQ campaign. We employed various evaluation statistics for this analysis: Pearson Correlation Coefficient (R), Root Mean Square Error (RMSE), Mean Bias (MB), Normalized Mean Bias (NMB), and Index of Agreement (IOA), all of which are defined below (Eq. 1–Eq. (5)).

$$R = \frac{\sum_{i=0}^{N}(Mod_i - \overline{Mod})(Obs_i - \overline{Obs})}{\sqrt{\sum_{i=1}^{N}(Mod_i - \overline{Mod})^2}\sqrt{\sum_{i=1}^{N}(Obs_i - \overline{Obs})^2}}, \quad \text{(Eq. 1)}$$

$$RMSE = \sqrt{\frac{\sum_{i=1}^{N}(Mod_i - Obs_i)^2}{N}}, \quad \text{(Eq. 2)}$$

$$MB = \frac{\sum_{i=1}^{N}(Mod_i - Obs_i)}{N}, \quad \text{(Eq. 3)}$$

$$NMB = \frac{\sum_{i=1}^{N}(Mod_i - Obs_i)}{\sum_{i=1}^{N}Obs_i}, \quad \text{(Eq. 4)}$$

$$IOA = 1 - \left[\frac{\sum_{i=1}^{N}(Mod_i - Obs_i)^2}{\sum_{i=1}^{N}(|Mod_i - \overline{Obs}| + |Obs_i - \overline{Obs}|)^2}\right]. \quad \text{(Eq. 5)}$$

3.1. Sensitivity of different meteorological inputs

We investigated the importance of meteorological input fields and their sensitivity in CTMs using two types of data: the Global Forecast System (GFS) and the Final (FNL) analysis data from the National Center for Environmental Prediction (NCEP). The GFS is a numerical weather prediction model that provides a global forecast of various meteorological variables, including temperature, pressure, wind, and precipitation. In contrast, the FNL represents a meteorological input field that merges observations from multiple sources with numerical model outputs, resulting in a comprehensive gridded dataset of atmospheric conditions for weather analysis.

The ensemble results of the five models, driven by both GFS and FNL data, are presented in Fig. 3, which shows the daily average timeseries for $PM_{2.5}$ and O_3. The corresponding performance evaluation results are displayed in Table 4. Utilizing FNL data improved simulating the temporal variations of $PM_{2.5}$ concentrations, with the R-value increasing from 0.84 to 0.94. Furthermore, compared to the use of GFS data, the NMB for $PM_{2.5}$ decreased from 22% to 11% with FNL data, indicating a reduced overestimation. Notably, the overestimation was significantly reduced from November 4 to 5 (Period 1) with FNL data. Fig. 3(a) illustrates the remarkable improvement observed when simulating the high concentration events of November 19–20 (Period 2) when using FNL data instead of GFS data.

To assess the meteorological variables that might be more sensitive

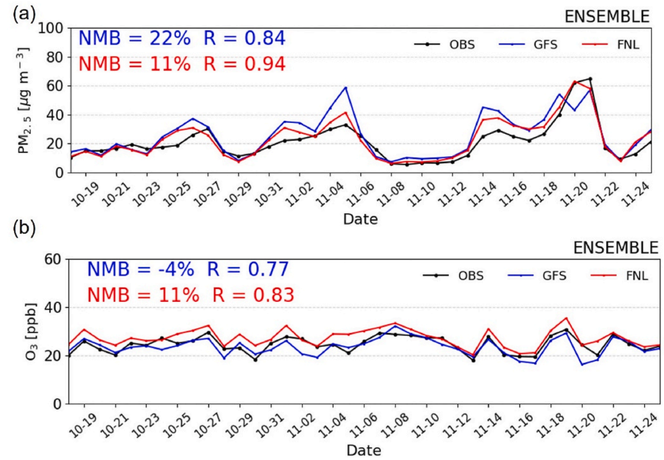

Fig. 3. Time series of ensemble results from models and $PM_{2.5}$ and O_3 mean concentrations observed daily at 505 Air-Korea stations. NMB and R indicate Normalized Mean Bias and Correlations, respectively.

Table 4
Performance evaluation of ensemble results from models by comparing the simulated concentration to the measured values for $PM_{2.5}$ and O_3 at 505 Air-Korea sites. Values in brackets represent average observations for each pollutant.

Pollutants	Input	R	RMSE	MB	NMB (%)	IOA
$PM_{2.5}$ (20.9 μg m^{-3})	GFS	0.84	9.16	4.62	22.12	0.88
	FNL	0.94	5.27	2.23	10.65	0.96
O_3 (24.58 ppb)	GFS	0.77	2.57	−0.95	−3.85	0.86
	FNL	0.83	3.37	2.69	10.94	0.79

to the $PM_{2.5}$ concentration performance, we compared surface and 850 hPa wind speeds and the planetary boundary layer height (PBLH) between the FNL and GFS datasets. During Period 1, the GFS data showed weaker surface wind speeds and a lower PBLH than the FNL data (as shown in Fig. S1), leading to an accumulation of $PM_{2.5}$ and, consequently, to an overestimation of its concentrations. In contrast, during Period 2, although wind speed and direction were similar between both meteorological input fields, a significant decrease in the PBLH was observed using the FNL data (as indicated in Fig. S2), which restricted the dispersion of $PM_{2.5}$ within the Korean Peninsula. As a result, the CTMs utilizing FNL data as the meteorological input were more successful in simulating the high-concentration events of $PM_{2.5}$ during Period 2. Previous studies have also confirmed that wind speed and PBLH are critical meteorological variables affecting pollutant concentrations (Jeong and Park, 2013; Li et al., 2014; Tao et al., 2018).

For O_3, the R-values were 0.77 for GFS and 0.83 for FNL. Similar to $PM_{2.5}$, the ensemble results showed a superior simulation of temporal changes when using FNL data. However, the NMB indicated an underestimation of approximately −4% with GFS data, whereas an overestimation of approximately 11% was recorded with FNL data, as illustrated in Fig. 3(b). These differences can be attributed to the surface air temperature from the meteorological inputs. An analysis of the spatial distribution of average 2 m temperature (TEMP2) throughout the GMAP/SIJAQ campaign period revealed that the FNL data corresponded to higher average temperatures (Fig. S3) than the GFS data. This effect can be associated with increased simulated O_3 concentrations, consistent with previous studies (Banta et al., 2011; Ramsey et al., 2014).

During the GMAP/SIJAQ campaign period, GFS forecasting data were used to pre-determine flight observation pathways and support the planning of various remote observations. Nevertheless, the primary objective of this study was to enhance the accuracy and performance of the CTMs via a comparative validation using data gathered during the comprehensive field campaign. The FNL is a re-analysis product generated after the completion of the GFS forecast cycle, incorporating the most comprehensive set of meteorological observations available for that cycle. We also demonstrated that CTM simulations driven by the FNL meteorological field yielded considerably better results than those using GFS data. Considering all these factors, the FNL re-analysis products were selected as the meteorological input field for conducting CTM simulations in this study.

3.2. Uncertainty in five different CTMs

The KORUS-AQ campaign, jointly conducted by U.S. NASA and South Korea NIER in 2016, was crucial for advancing our understanding of air quality characteristics in the Northeast Asia region and the Korean Peninsula. The subsequent GMAP/SIJAQ campaign was expected to provide detailed and intensive observational data that was not easily obtained through regular monitoring, thereby contributing significantly to emission estimations and model performance improvements.

We first compared the ground-level concentrations of air pollutants obtained from 505 Air-Korea sites and the Olympic Park special observation site with the results from five different models that used FNL data. We also examined the ensemble results generated by these models and compared them to the model results from the previous KORUS-AQ campaign (Park et al., 2021). However, the GMAP/SIJAQ campaign was conducted from October to November, and the KORUS-AQ campaign was conducted from May to June, which makes it challenging to compare the modeling results directly due to the differing seasonal contexts. Seasonal variations significantly impact atmospheric conditions, pollutant sources, and meteorological patterns, which can, in turn, influence model performance. However, notably, in various air quality modeling studies in Korea, modeling results for seasons other than winter have demonstrated similar performances (Choi et al., 2019, Ju et al., 2018). The seasonal characteristics of ambient $PM_{2.5}$ in Korea exhibit similar concentration levels in both spring and fall. However, the impact of Transboundary air pollution (TAP) on $PM_{2.5}$ concentrations is approximately 6% higher in spring compared to that in fall (Yim et al., 2019). Inland, the concentration of $PM_{2.5}$ is approximately 5–7 μg m^{-3} higher in spring than in autumn, but the diurnal pattern is similar. Despite the inherent seasonal differences, it was considered likely that a comparative analysis of the GMAP/SIJAQ and KORUS-AQ campaign results could yield meaningful insights. By acknowledging the seasonal context and leveraging the generally higher accuracy of spring and autumn time modeling, we derived valuable conclusions about model performances and the underlying atmospheric processes. Therefore, while direct comparisons are fraught with complexities, the analysis results are useful for enhancing our understanding of model performance across different campaigns and seasons.

Similar to the validation of the model performance during the KORUS-AQ campaign, validation of the GMAP/SIJAQ campaign was

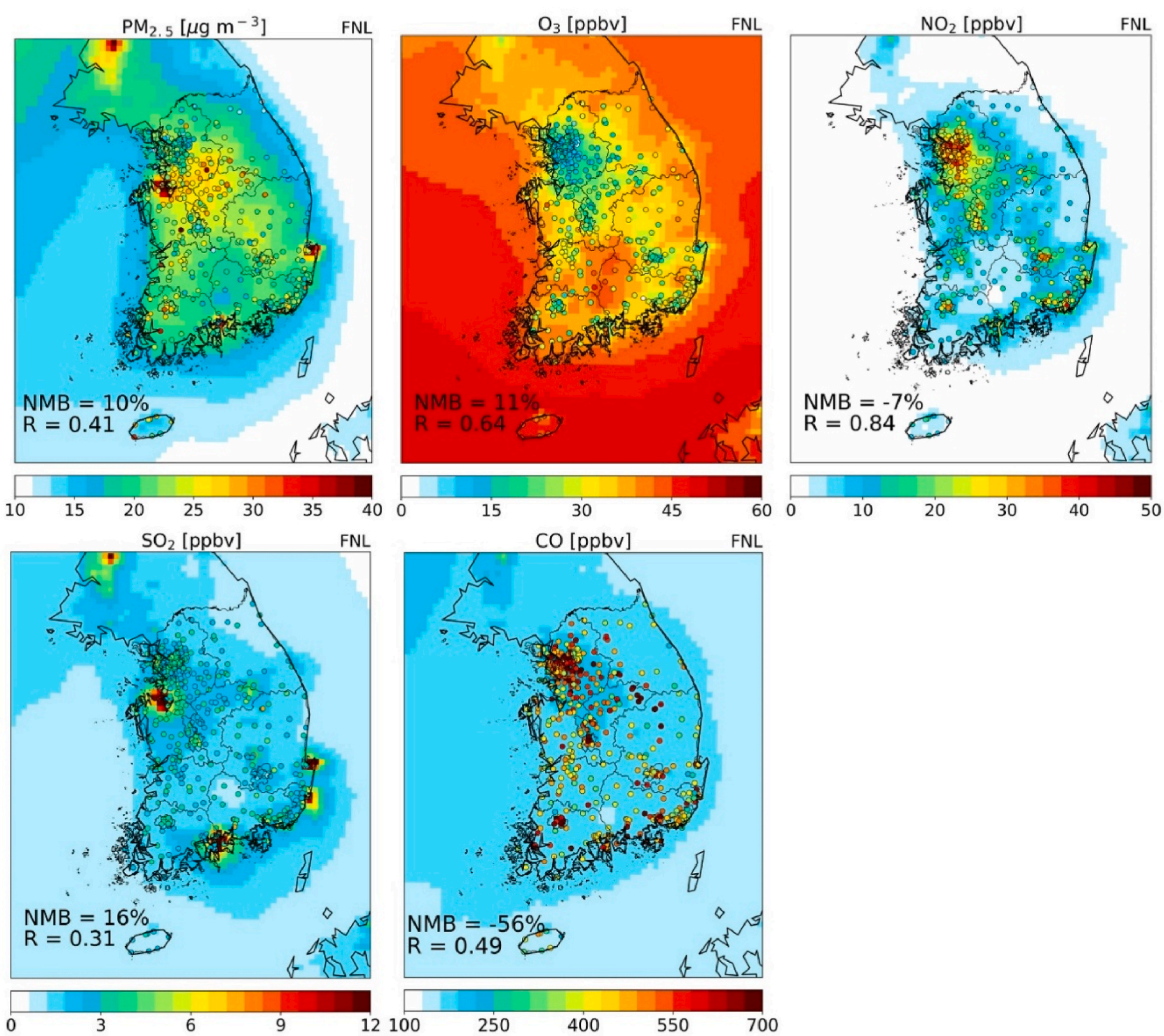

Fig. 4. A model ensemble obtained using FNL meteorological input fields and observed mean values of $PM_{2.5}$, O_3, NO_2, SO_2, and CO surface concentration during the GMAP campaign (October 18 to November 25, 2021). The background represents model values, and circles indicate the location of 505 Air-Korea surface monitoring stations and their observed values.

performed using observational data from Air-Korea monitoring stations, focusing on South Korea. During the KORUS-AQ campaign, two global models, GEOS-Chem and CAM-Chem, and six regional models were utilized. These included WRF-Chem from NCAR, WRF-Chem from Pusan National University, WRF-Chem from the University of Iowa, WRF-Chem from UCLA, and CMAQ (Park et al., 2021). In this study, we used five CTMs, including WRF_GC, WRF-Chem, CMAQ, CMAQ_G, and CAMx. Fig. 4 compares the spatial distribution of the average observed values and the ensemble results for $PM_{2.5}$, O_3, NO_2, SO_2, and CO obtained from the five models during the GMAP/SIJAQ campaign period. Compared to the model results from the previous KORUS-AQ campaign (Park et al., 2021), the model performances for $PM_{2.5}$, O_3, and NO_2 were improved. For $PM_{2.5}$ and O_3, the spatial correlation increased from 0.17 to 0.41 and 0.55 to 0.67, respectively, indicating a better representation of the spatial distribution than that observed in the KORUS-AQ modeling study.

For NO_2, the spatial correlation was nearly the same as that recorded during the KORUS-AQ campaign, but the Normalized Mean Bias (NMB) was significantly reduced from −27% to −7%, indicating that this modeling significantly improved the underestimation issue encountered during the KORUS-AQ modeling. The improved model performance can be attributed to updates in the emission inventory for NO_X, advancements in the model version, and implementation of much higher horizontal resolutions in GMAQ/SIJAQ modeling. To assess the improvement in model performance due to resolution, we interpolated the 9 km × 9 km domain to 0.5° × 0.5° and examined the results (Fig. S4, Table S1). For $PM_{2.5}$ and O_3, the spatial correlation increased from 0.17 to 0.54 and 0.55 to 0.70, respectively. For NO_2, the NMB was slightly reduced from −27% to −25%. These findings indicate that the model performance improved even when evaluated at the same resolution.

Despite the overall improvement in model performance when compared to the KORUS-AQ period, a few variables showed limited improvement. Notably, for SO_2, an unexpected degradation in modeling performance was noted, i.e., a decrease in the spatial correlation from 0.74 to 0.31 (0.5°; 0.74 to 0.23). For CO, the NMB value deteriorated from −47% to −56% (0.5°; −47% to −58%), indicating an increased underestimation. Previous studies of the KORUS-AQ campaign have also reported that CTMs underestimate CO concentrations in Korea (Gaubert et al., 2020; Huang et al., 2018; Tang et al., 2019). Similar results were obtained in the GMAP/SIJAQ campaign, suggesting that sources of CO emissions estimates may be missing, potentially leading to an underestimation of CO ground concentrations.

Fig. 5 shows the time series of daily averaged modeled values and observed values during the GMAP/SIJAQ campaign, and the statistical results for each pollutant and model are presented in Table 5. Despite the presence of discrepancies among the models and performance variations based on the pollutant, the ensemble results for $PM_{2.5}$ generally exhibited better performance than the individual models, showing a

Table 5
Performance evaluation of the four models (five types for $PM_{2.5}$) and their ensemble by comparing the simulated concentration to the measured values at 505 Air-Korea sites for $PM_{2.5}$ O_3, NO_2, SO_2, and CO. Values in bracket represent the average observations for each pollutant.

Pollutants	Model	R	RMSE	MB	NMB (%)	IOA
$PM_{2.5}$ (20.9 μg m^{-3})	CMAQ	0.95	5.39	−3.41	−16.29	0.95
	CMAQ_G	0.97	4.96	2.68	12.81	0.97
	CAMx	0.94	11.03	8.25	39.49	0.88
	WRF_Chem	0.79	9.56	−5.24	−25.08	0.80
	WRF_GC	0.81	15.33	9.30	44.50	0.78
	ENSEMBLE	0.94	5.27	2.23	10.65	0.96
O_3 (24.58 ppb)	CMAQ	0.76	2.72	−1.23	−5.02	0.84
	CMAQ_G	0.70	6.90	5.34	21.73	0.59
	CAMx	0.59	3.03	0.18	0.75	0.76
	WRF_GC	0.66	7.46	6.59	26.80	0.52
	ENSEMBLE	0.83	3.37	2.69	10.94	0.79
NO_2 (18.75 ppb)	CMAQ	0.87	4.29	3.44	18.35	0.83
	CMAQ_G	0.92	2.66	−1.71	−9.14	0.93
	CAMx	0.89	2.24	−0.34	−1.82	0.94
	WRF_GC	0.66	7.84	−6.73	−35.87	0.60
	ENSEMBLE	0.87	2.79	−1.30	−6.93	0.91
SO_2 (2.82 ppb)	CMAQ	0.70	0.85	−0.15	−5.20	0.48
	CMAQ_G	0.72	0.84	−0.04	−1.48	0.49
	CAMx	0.73	2.26	1.76	62.36	0.18
	WRF_GC	0.71	0.99	0.23	8.34	0.44
	ENSEMBLE	0.74	1.07	0.45	15.93	0.41
CO (447.46 ppb)	CMAQ	0.91	302.61	−296.26	−66.21	0.34
	CMAQ_G	0.95	224.37	−222.20	−49.66	0.47
	CAMx	0.85	277.34	−272.22	−60.84	0.38
	WRF_GC	0.82	223.91	−216.98	−48.49	0.46
	ENSEMBLE	0.91	218.62	−215.97	−54.97	0.43

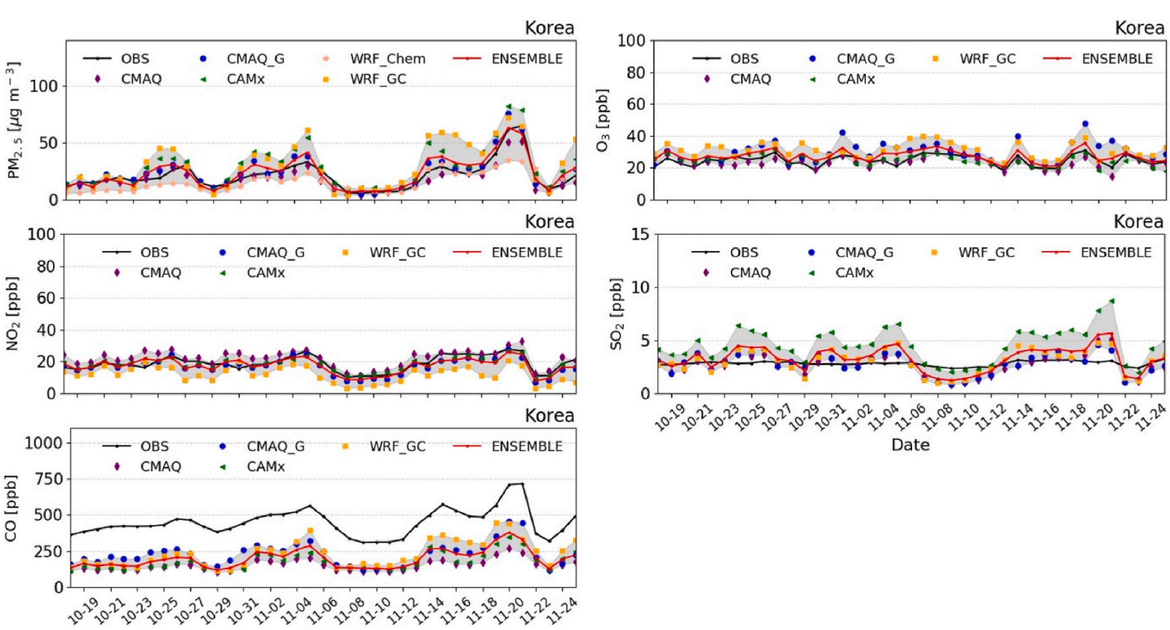

Fig. 5. Time series of simulated and mean concentrations of $PM_{2.5}$, O_3, NO_2, SO_2, and CO at 505 observed daily at Air-Korea stations. The black and red lines represent the observed and ensemble simulated values. The marker indicates the simulated value of each model, and model ranges are shown in gray shades.

high R-value of 0.94 and a low NMB of 11%, consistent with previous studies (Baklanov and Zhang, 2020; Marécal et al., 2015). Moreover, compared to the model results from the KORUS-AQ campaign (Park et al., 2021), a much wider variation and improvement in performance among the models was observed for $PM_{2.5}$, with R-values ranging from 0.72 to 0.81 for KORUS-AQ and 0.79 to 0.97 for GMAP/SIJAQ. This improvement can be attributed to the newly added ensemble member in this study, the CMAQ_G model, which exhibited a significantly better performance than the other models that showed similar performances during the KORUS-AQ campaign. CMAQ_G is a version of CMAQ (version 5.2.1) optimized for the Korean peninsula (Yu et al., 2023), and it includes major updates such as revised daytime HONO chemistry, updated yields for Secondary Organic Aerosol (SOA) formation and the application of 3D-Var data assimilation. This enhanced performance was particularly notable for $PM_{2.5}$, with an R-value of 0.97 and an NMB of 13%, compared to the ensemble results (R = 0.94; NMB = 11%). These results may highlight the importance of adopting region-specific and optimized models, which can deliver improved performance in modeling outcomes and assist in an in-depth understanding of air pollution phenomena and mechanisms over the target region.

For NO_2 and O_3, the CMAQ model exhibited a distinct pattern compared to other models, with an overestimation of NO_2 and an underestimation of O_3. Despite using the same emission inventories as other models, the in-line calculation of the CMAQ model for point source emissions caused such differences. In the CMAQ model, point source emissions can be optionally handled using in-line calculation, which was used in the CMAQ employed in this study. Hence, the emissions were directly integrated into the dynamic processes of the model during the simulation run. Specifically, point source emissions, such as those from industrial facilities or power plants, were injected into the relevant model grid cells at their respective heights based on the stack parameters (e.g., stack height, exit velocity, and temperature). In contrast, the other models often used a pre-processing step to allocate emissions to vertical layers before the simulation began.

In the case of SO_2, the ensemble results generally demonstrated a strong performance with an R-value of 0.74 and an NMB of 16%. However, a detailed examination of the time series revealed that the model overestimated the variability compared to the observed data, and this discrepancy appears to be linked to inaccuracies in the emission inventory for industrial regions. For example, while the model effectively captured observations in Baengnyeong Island, a background area with minimal local sources, it failed to accurately represent both the concentration levels and variability in Ulsan, an industrial area. This issue is illustrated in Fig. S5.

Furthermore, the CAMx model showed an R-value of 0.73 and an NMB value of 62%, indicating a significant overestimation compared to the other models. The approach of CAMx to vertical mixing, particularly via the dynamic adjustment of the vertical diffusivity (Kv) and its robust parameterization schemes, results in stronger and more responsive vertical mixing than other models such as WRF-Chem, CMAQ, and WRF_GC. A previous study by Vivanco et al. (2017) reported similar characteristics with CAMx. Pirovano et al. (2012) also argued that the CAMx model was distinguished by its notably strong downward mixing tendency compared to other models, resulting in an increased impact of elevated sources on ground-level concentrations, especially in the case of SO_2.

The results of a comprehensive examination of the model validation for simulated CO concentrations are shown in Figs. 4 and 5, and Table 5, and they highlight the need for future scientific research. The strong correlation (R = 0.91) between the simulated CO concentration of the model ensemble using SIJAQv2 emissions and observed concentrations in Air Korea stations indicates that the model ensemble accurately captured temporal variations in the CO concentration. However, the significant difference between simulated CO concentrations and observed concentrations (NMB = −55%) indicates a consistent underestimation by the model ensemble. In the previous study of the KORUS-AQ campaign, the issue of underestimating the CO concentration persisted despite applying the updated KORUSv5 inventory, which more than doubled the CO emission amounts compared to KORUSv1. The underestimation of CO concentrations across all models is likely due to a combination of challenges in accurately representing anthropogenic sources and the inherently low background CO levels in the models. This underestimation is consistently observed across various regions, including urban areas like Seoul, suburban locations such as Hongcheon, and background sites like Baengnyeong (Fig. S6). The underestimation in urban regions suggests that significant sources of CO emissions, such as traffic, industrial activities, and residential heating, may not be fully captured in the emissions inventory. In contrast, the underestimation observed in Baengnyeong, where local emissions are minimal, suggests that the model's tendency to underestimate natural background CO levels, rather than missing local sources, may be the primary factor in these areas. This consistent pattern of underestimation across diverse geographical settings implies a systematic bias in the representation of baseline CO concentrations by models, contributing to the overall negative bias. Addressing these issues would require enhancements in both the emissions inventory to better account for anthropogenic sources and the model's abilities to represent background CO levels more accurately. Gaubert et al. (2020) also showed that chemical production and loss resulting from OH reactions caused by the release of VOCs have a significant impact on CO concentration simulations. This implies that in addition to improving emissions accuracy, CTMs must more accurately capture the complex chemical processes that may influence CO concentrations.

Fig. 6 demonstrates the modeled and observed values of the diurnal cycles of various pollutants. The diurnal patterns of air pollutants vary significantly (Choi et al., 2023; Liu et al., 2022; Yoo et al., 2015). SO_2 and O_3 typically exhibit a single peak in their daily concentrations. In contrast, pollutants such as $PM_{2.5}$, CO, and NO_X tend to exhibit a bimodal distribution, with two distinct peaks occurring in the morning and evening. These patterns are primarily influenced by traffic emissions and atmospheric processes, reflecting the daily human activities and meteorological conditions that affect pollutant levels throughout the day. For $PM_{2.5}$, NO_2, and O_3, the models exhibited variations consistent with the observed data and captured the diurnal fluctuations well. However, the daytime peak concentration for O_3 and the early morning maximum for $PM_{2.5}$, NO_2, and SO_2 occurred approximately 2 h earlier than the observed timing in all model results. Additionally, the models were unable to accurately simulate the observed diurnal variations in SO_2. In the early 2000s, diurnal variations in SO_2 in Korea exhibited a bimodal pattern (Kim et al., 2007), whereas the diurnal variation distribution of SO_2 observed in this study showed a single peak. This change is believed to result from the decreased emissions from mobile pollution sources. According to the Clean Air Policy Support System (CAPSS; www.air.go.kr), which provides statistical information on emissions in Korea, the proportion of SO_2 emissions from mobile sources decreased from 9.39% in 1999 to 5.4% in 2021, and the proportion of road-mobile pollutants decreased from 1.18% to 0.15%. This indicates that SO_2 emissions from transportation, which contribute to the bimodal pattern, have been primarily eliminated. However, the temporal allocation of emissions used in the model inputs did not align well with observations, leading to discrepancies between model simulations and observations. This suggests the potential need for relevant correction in the temporal profile and allocation in the emission processing procedure. As mentioned earlier, all models underestimated CO concentrations, although its diurnal patterns were relatively well captured. The underestimation of variations in diurnal CO concentrations by CTMs suggests that sources of CO emissions estimates may be missing, particularly those of local sources.

The diurnal cycle of $PM_{2.5}$ can be comprehensively understood by examining the contribution of gaseous pollutants to its formation. During the morning rush hours, traffic activity significantly increases NO_2 emissions, peaking at around 09:00. NO_2 then reacts with OH radicals to

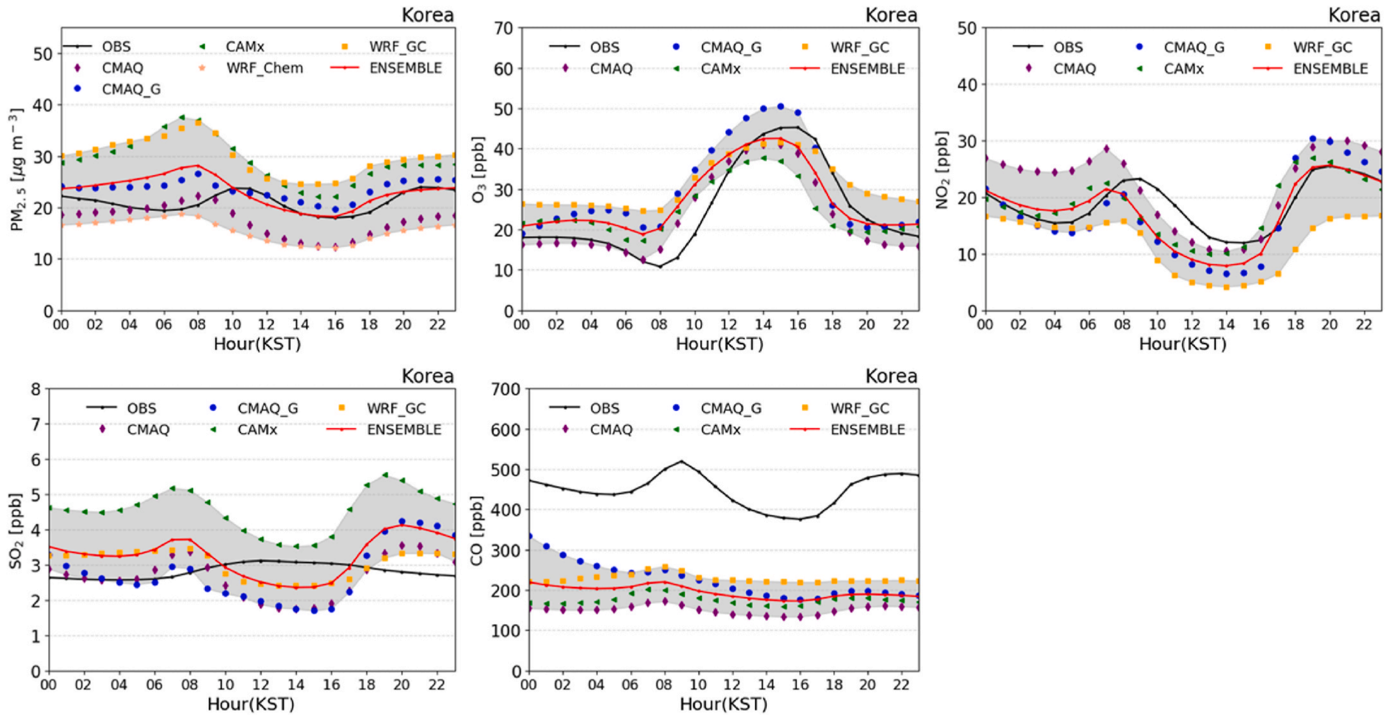

Fig. 6. Diurnal cycle of simulated and mean concentrations of $PM_{2.5}$, O_3, NO_2, SO_2, and CO observed daily at 505 Air-Korea stations. The black and red lines represent the observed and ensemble simulated values. The marker indicates the simulated value of each model, and model ranges are shown in gray shades.

form nitric acid, which subsequently condenses with ammonia (NH_3) to produce ammonium nitrate. Simultaneously, hydrocarbons, as indicated by the concentration of CO, also increased during this period, leading to the formation of hydrocarbon organic aerosols. Notably, the concentration of $PM_{2.5}$ reaches its morning peak around 11:00, approximately 2 h after the maxima of NO_2 and CO. This temporal lag suggests that the oxidation processes of NO_2 and hydrocarbons, along with subsequent particle formation, are completed within a few hours (Kim and Kim, 2020). This pattern aligns with the real-time observations reported in China by Wang et al. (2016), where similar diurnal dynamics were observed. This analysis highlights the complex interplay between gaseous precursors and particulate matter, emphasizing the role of secondary aerosol formation in shaping the diurnal cycle of $PM_{2.5}$. Understanding these temporal dynamics is crucial for developing targeted air quality management strategies and mitigating pollution peaks effectively.

Notably, while nighttime (00:00–06:00 KST) measurements indicated a decrease in $PM_{2.5}$ concentration, the models conversely showed increases in its concentration. The decrease in $PM_{2.5}$ concentrations at night can be attributed to the combined effects of meteorological changes, reduced emissions (human activities), and altered chemical processes (photochemical reactions) (Faisal et al., 2022; Han and Hong, 2020; Leung et al., 2020; Ye et al., 2017). Human activities contributing to $PM_{2.5}$ emissions, such as vehicular traffic and industrial operations, are significantly reduced during night hours, resulting in lower primary emissions. Furthermore, the absence of sunlight at night halts photochemical reactions that generate secondary pollutants from primary emissions, reducing the formation of secondary aerosols, a major component of $PM_{2.5}$. These factors collectively contribute to the observed decrease in $PM_{2.5}$ concentrations at night. However, since the models simulated increased $PM_{2.5}$ concentrations at night, an analysis of this discrepancy is necessary. A detailed discussion of this issue is presented in Section 3.3.

We also compared the ensemble results of the GMAP/SIJAQ campaign in this study with those of the KORUS-AQ campaign as presented in the existing literature (Park et al., 2021). For $PM_{2.5}$, the R-values increased from 0.88 to 0.94, indicating an improvement in simulating temporal variations. For O_3, although the R-value remained at 0.83, the NMB increased from 4% to 11%. Informed by the KORUS-AQ campaign's findings on air quality over Northeast Asia and the Korean Peninsula, numerous scientific and technical efforts have been made to refine modeling techniques, including correcting emission estimates and updating model physical and chemical options. As a result, the modeling performance for concentrations of air pollutants during the GMAP/SIJAQ campaign period improved noticeably.

Here are a few notable findings from this evaluation and comparison.

1. Due to emissions updates and model improvements, the overall model performances in this study were improved compared to the KORUS-AQ campaign.
2. Overall, the ensemble of models demonstrated a better performance than individual models during the GMAP/SIJAQ campaigns.
3. All models consistently underestimated CO concentrations, suggesting the possibility of missing sources in CO emission inventories.
4. While the models successfully captured diurnal variations, adjustments in the temporal profiles of the emissions processing procedure are necessary.

3.3. Biases associated with aerosol compositions

The $PM_{2.5}$ concentrations and aerosol chemical composition were measured every 4 h at Olympic Park. The results were averaged daily and compared to those of each model. During the GMAP/SIJAQ campaign period, Seoul experienced high concentrations of $PM_{2.5}$ (November 19–21, 2021). As shown in Fig. 7 (gray shades), significant model variations was observed during this period. Excluding the high concentration period, both CAMx and WRF_GC over simulated $PM_{2.5}$, whereas CMAQ clearly under-simulated $PM_{2.5}$ during the high concentration period. In WRF_GC, the underestimation of sulfate significantly affected the underestimation of $PM_{2.5}$ during high-concentration periods. However, the $PM_{2.5}$ concentration simulated by CMAQ_G during the high concentration period was most similar to that of observations,

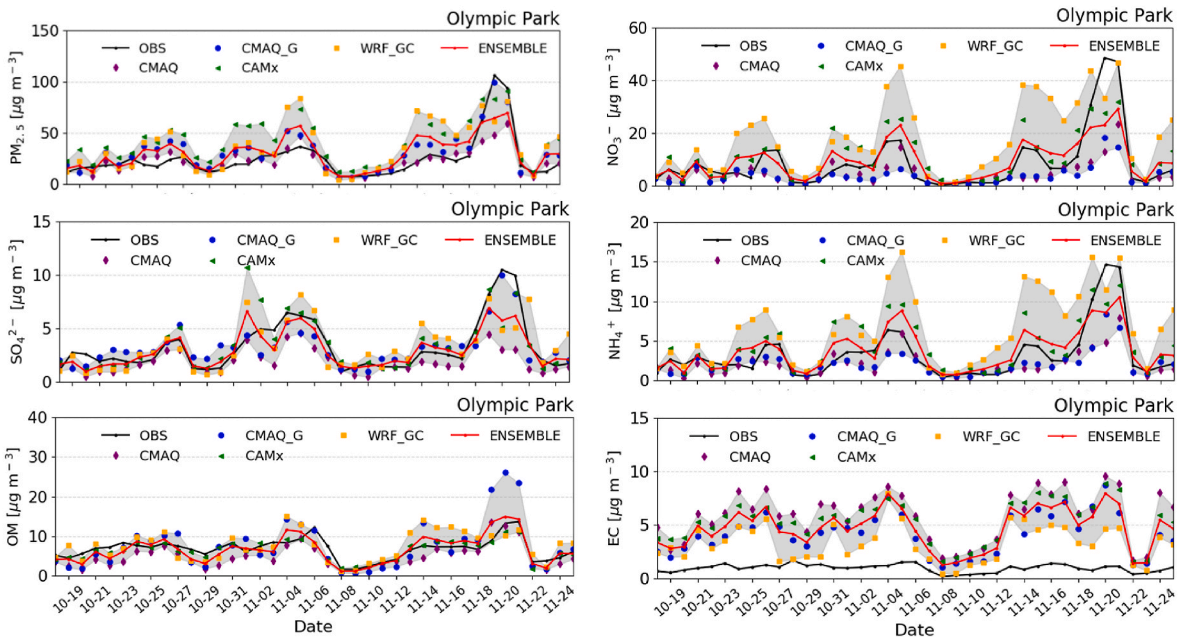

Fig. 7. Time series of simulated and observed concentrations of $PM_{2.5}$, NO_3^-, SO_4^{2-}, NH_4^+, OM, and EC observed daily at Olympic Park in Seoul, Korea. The black and red lines represent the observed and ensemble simulated values, respectively. The marker indicates the simulated value of each model, and model ranges are shown in gray shades.

and this was primarily due to data assimilation for $PM_{2.5}$. These discrepancies highlight the need for further refinement in model chemical processes and data assimilation techniques to improve simulation accuracy across different atmospheric conditions.

Jordan et al. (2020) and Travis et al. (2022) explored the challenges in accurately simulating $PM_{2.5}$ concentrations during high pollution periods with atmospheric models, focusing on the KORUS-AQ campaign. Jordan et al. (2020) identified significant discrepancies in the GEOS-Chem model's ability to simulate the chemical composition of $PM_{2.5}$, noting an underestimation of sulfate and an overestimation of nitrate due to missing heterogeneous chemistry in aerosol liquid water and an incorrect representation of nighttime chemistry. Travis et al. (2022) attributed the overestimation of nitrate concentrations to several key model failures, including the overestimation of daytime nitric acid levels, the incorrect representation of nighttime chemistry, and an overly shallow and insufficiently turbulent nighttime mixed layer. These inaccuracies exacerbated the model's inability to simulate the buildup of $PM_{2.5}$ during haze pollution events.

The WRF_GC model tended to overestimate nitrate and ammonium concentrations, which do not vary between day and night (Fig. S7). An overestimation of OM was predominantly observed at night. In contrast, the CMAQ_G model tended to overestimate OM during the day. Several studies (Jeong and Kim, 2021; Schnell et al., 2018) have suggested that underestimating the PBLH could contribute to nighttime overestimations. In this respect, the YSU scheme underestimates nighttime PBLH compared to other PBL schemes (Fig. S8). The characteristics of the various PBL schemes and their differences are detailed in the study of Liu et al. (2023). Therefore, using different PBL approaches could improve simulations of high nighttime concentrations, the simulated nighttime concentration levels varied across models despite all models using the same YSU scheme, indicating that other factors may play a more significant role than the PBLH. This suggests that differences in the chemical processes within each model are particularly influential. As a considerable amount of research on atmospheric chemical processes has been covered in preceding studies, this section examines the roles of various meteorological factors.

Fig. S7 illustrates the diurnal variations in $PM_{2.5}$ components observed at Olympic Park. The observational data indicate increases in the concentrations of all substances from 00:00 to 08:00 KST, which were successfully simulated by the model ensemble. However, as previously mentioned, the observational results for Korea revealed that the models did not accurately simulate the decrease in concentration during nighttime. Due to several factors, diurnal variations in pollutants can differ significantly between specific regions and the broader country. Local emission sources, such as traffic and industrial activities, create distinct diurnal patterns, especially in urban areas with pronounced peaks during rush hours. Meteorological conditions, including wind patterns and temperature inversions, influence pollutant dispersion differently in various regions (Dominick et al., 2012; Lennartson et al., 2018). Uniform temporal patterns applied nationally in air quality models can lead to discrepancies, as this approach fails to accurately capture local variations. Conversely, applying urban patterns to these models may not accurately reflect nationwide changes. Although diurnal pollutant patterns can differ due to factors such as local emissions, meteorological conditions, and emission patterns, further research is needed to explain the differences in diurnal patterns between the region and the country observed during this campaign.

When comparing chemical components, the variations among models were even greater than those observed when comparing total mass concentration, especially for high-concentration periods. Fig. 8 and Table 6 show scatter plots and statistics reflecting differences between the ground observations and model results.

During the campaign, the CMAQ model generally simulated $PM_{2.5}$ concentrations well, but it underestimated them during high-concentration periods. This underestimation is likely due to biases in the meteorological model (WRF), particularly inaccurate precipitation events. The model showed that significant precipitation occurred during the high concentration period (Fig. S9(a)), but no actual precipitation was observed. Excluding the high concentration period, MB for $PM_{2.5}$ concentrations improved from −2.28 $\mu g/m^3$ to −0.68 $\mu g/m^3$, and the NMB improved from −9.26% to −3.51%.

In the case of CMAQ and CMAQ_G, the NO_3^- concentration was underestimated, with RMSE values of 8.85 $\mu g\ m^{-3}$ and 9.35 $\mu g\ m^{-3}$, respectively. This underestimation is also attributed to the model's inability to accurately simulate the heterogeneous chemical reaction of nitrate during the high concentration period. When the model

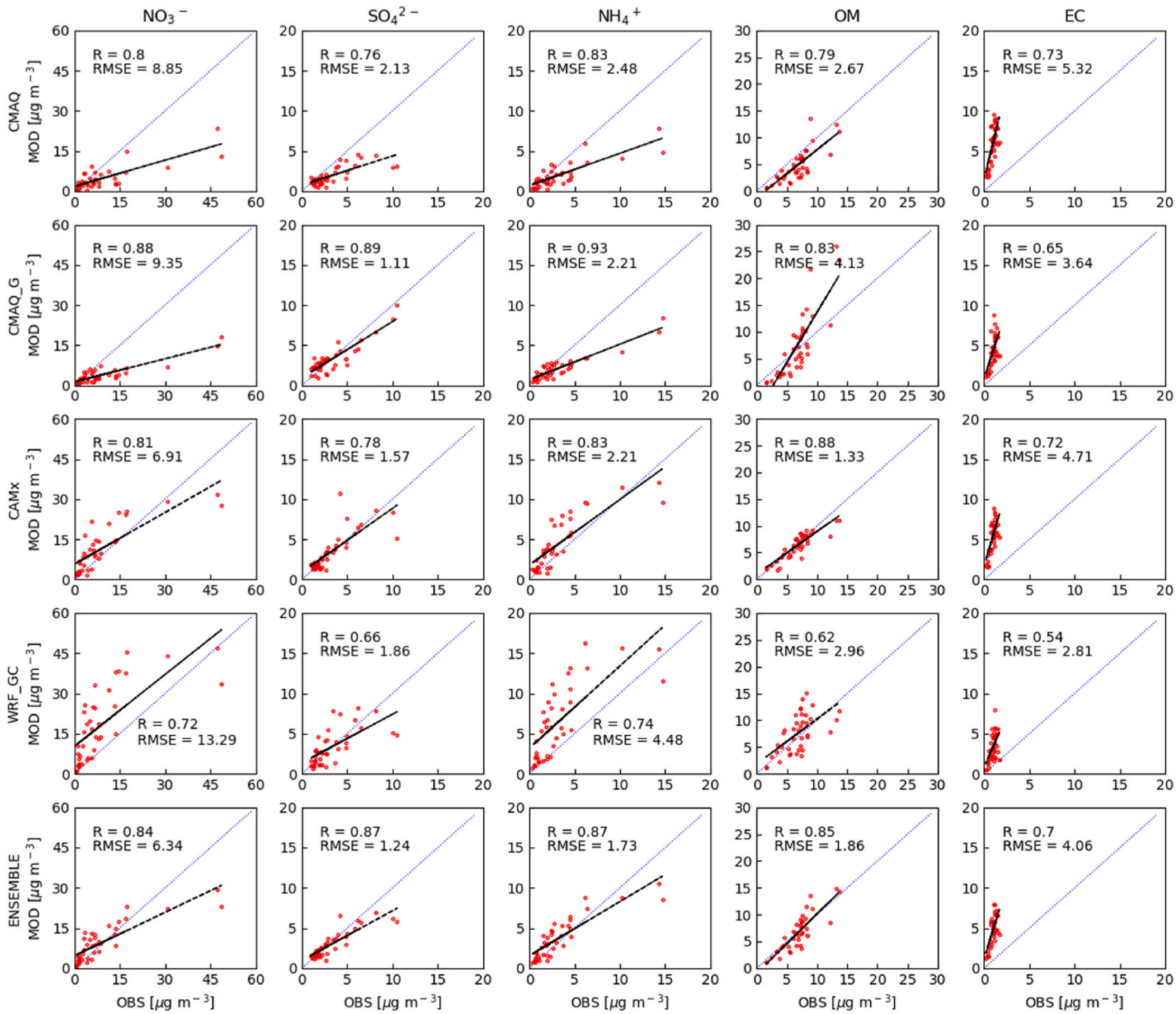

Fig. 8. Scatter plots of simulated and mean concentrations of NO_3^-, SO_4^{2-}, NH_4^+, OM, and EC recorded daily at Olympic Park in Seoul, Korea.

performance was evaluated after excluding the high concentration period, the RMSE values improved to 4.52 μg m^{-3} and 4.86 μg m^{-3}, respectively, which were half of the RMSE of the entire campaign period. Nonetheless, NO_3^- was still underestimated by CMAQ and CMAQ_G (MB; −2.15 μg m^{-3} to −2.81 μg m^{-3}), and this can be attributed to a variety of causes. One possible explanation is that during the campaign period, relative humidity (RH) was rather underestimated by the WRF models, as shown in Fig. S9(b). This underestimation of RH may have led to lower of NO_3^-, SO_4^{2-}, and NH_4^+ compound production rates (Sun et al., 2022). Additionally, uncertainties in the chemical mechanism of the current CMAQ model for secondary inorganic production, including missing or inadequately represented heterogeneous reactions, along with uncertainties in NO_X and NH_3 emissions, could be responsible for this discrepancy (Kong et al., 2020; Qiao et al., 2015; Shimadera et al., 2014; Xie et al., 2022; Zheng et al., 2020).

For OM, all the models and the ensemble results simulated the observed values quite well. While CMAQ_G overestimated OM compared to observations, the RMSE values improved from 4.13 μg m^{-3} to 2.54 μg m^{-3}, excluding high concentration periods (Table 6 and Table S1). The observed concentrations of OM in the $PM_{2.5}$ samples ranged from 1.56 to 13.62 μg m^{-3} (with a mean of 6.74 ± 2.65 μg m^{-3}) during the campaign period, as averaged OM constituted approximately 27% of the total $PM_{2.5}$ mass. According to Hussein et al. (2022), the observed concentrations of annual mean OM in Asia are 5.9 ± 2.8 μg m^{-3}. While the ratio of OM to $PM_{2.5}$ (27%) was slightly higher than that observed in other Asian cities, such as Shanghai at 18% during 2006–2007, Beijing at 23% in 2000, and Amman at 13% during 2018–2019 (Hou et al., 2011; Hussein et al., 2022), notably, both observed OM concentrations and those modeled in this study were comparable to those recorded in other studies.

However, all models overestimated EC, with MB values ranging from 2.34 μg m^{-3} to 4.92 μg m^{-3}, which were even higher than the observed concentrations during the campaign period (from 0.17 to 1.68 μg m^{-3} with a mean of 0.95 ± 0.37 μg m^{-3}). Moreover, the observed concentrations of annual mean EC in the Asian region were reported as 1.7 ± 1.1 μg m^{-3} according to a previous study (Hussein et al., 2022). This huge discrepancy in EC concentrations is mainly attributed to the overestimation of EC emission amount in the SIJAQv2 inventory. Primary sources of EC include direct emissions from mobile sources and biomass burning. Overall, EC emissions from the Korean Peninsula have

Table 6
Performance evaluation of the four types of models and their ensemble by comparing the simulated concentration to the measured values for $PM_{2.5}$, NO_3^-, SO_4^{2-}, NH_4^+, OM, and EC at Olympic Park in Seoul, Korea. Values in the bracket represent the average observations for each pollutant.

Pollutants	Model	R	RMSE	MB	NMB (%)	IOA
$PM_{2.5}$ (24.61 μg m^{-3})	CMAQ	0.82	12.68	−2.28	−9.26	0.83
	CMAQ_G	0.90	10.81	6.19	25.14	0.93
	CAMx	0.76	23.13	18.16	73.76	0.73
	WRF_GC	0.63	21.98	11.51	46.76	0.73
	ENSEMBLE	0.80	13.39	5.4	21.93	0.86
NO_3^- (8.65 μg m^{-3})	CMAQ	0.80	8.85	−4.07	−47.06	0.68
	CMAQ_G	0.88	9.35	−4.83	−55.78	0.64
	CAMx	0.81	6.91	2.67	30.87	0.87
	WRF_GC	0.72	13.29	9.36	108.16	0.73
	ENSEMBLE	0.84	6.34	0.70	8.14	0.87
SO_4^{2-} (3.25 μg m^{-3})	CMAQ	0.76	2.13	−1.33	−40.84	0.66
	CMAQ_G	0.89	1.11	−0.02	−0.74	0.93
	CAMx	0.78	1.57	0.24	7.37	0.88
	WRF_GC	0.66	1.86	0.08	2.61	0.80
	ENSEMBLE	0.87	1.24	−0.27	−8.25	0.90
NH_4^+ (3.23 μg m^{-3})	CMAQ	0.83	2.48	−1.24	−38.52	0.74
	CMAQ_G	0.93	2.21	−1.10	−34.00	0.80
	CAMx	0.83	2.21	1.20	37.13	0.88
	WRF_GC	0.74	4.48	3.24	100.52	0.71
	ENSEMBLE	0.87	1.73	0.50	15.43	0.91
OM (6.74 μg m^{-3})	CMAQ	0.79	2.67	−1.93	−28.67	0.8
	CMAQ_G	0.83	4.13	0.79	11.8	0.76
	CAMx	0.88	1.33	−0.38	−5.59	0.93
	WRF_GC	0.62	2.96	0.76	11.22	0.74
	ENSEMBLE	0.85	1.86	−0.2	−3.04	0.9
EC (0.95 μg m^{-3})	CMAQ	0.73	5.32	4.92	517.53	0.11
	CMAQ_G	0.65	3.64	3.22	338.66	0.16
	CAMx	0.72	4.71	4.39	462.11	0.13
	WRF_GC	0.54	2.81	2.34	246.59	0.19
	ENSEMBLE	0.70	4.06	3.72	391.18	1.14

been declining since 2016, according to KORUSv5 and SIJAQv2 emissions. However, EC emission amounts near Olympic Park, where an intensive monitoring station was located for this study, were approximately 3.2-fold higher than average amounts for the Korean peninsula. The abnormally elevated EC emissions in the SIJAQv2 inventory are likely due to unusual emission sources, such as the temporary construction activities in this area in 2018. Although the SIJAQv2 inventory was based on data from 2018, the GMAP/SIJAQ campaign in this study was conducted in 2021. Therefore, it can be concluded that an overestimation of EC occurs in all models utilized.

Overall, variations in the aerosol composition were more significant among the models than those of total $PM_{2.5}$ concentration, and such variations were particularly evident during the higher concentration period. Notably, inadequacies in the simulation of meteorological variables, such as precipitation, relative humidity, and PBLH, led to increased uncertainty in the simulation of pollutant concentrations. Similar to the findings in Section 3.2, the collective performance of the ensemble result was superior, and the simulation for all aerosol chemical compositions, with the exception of EC, was also remarkable.

4. Conclusions

An intensive field campaign, GMAP/SIJAQ 2021, was conducted in Korea from October to November 2021 to advance the development of the GEMS algorithm, ensure the accuracy of its products, and enhance our understanding of air pollution on the Korean Peninsula. Air quality forecasting by five different CTMs was utilized to plan the observation schedule for the campaign. In this study, the performance of five different CTMs (and their ensemble) was assessed using intensive measurement data during the campaign period to understand the characteristics of each CTM and identify their strengths and limitations in simulating air quality.

To assess the impact of meteorological input data on CTM accuracy, we conducted simulations using two different meteorological datasets, GFS and FNL. The results indicated that the model's performance in predicting $PM_{2.5}$ and O_3 concentrations significantly improved when utilizing FNL data, with R-values ranging from 0.84 to 0.94 for $PM_{2.5}$ and 0.77 to 0.83 for O_3. Moreover, the model even more accurately captured high-concentration events, whereas it tended to overestimate O_3 levels (NMB: 4%–11%) with the FNL data compared to that observed with the GFS data.

The performance of ensemble simulations in this study was compared to that using previous KORUS-AQ 2016 campaigns, and an improvement was noted. The temporal correlation for total mass concentrations of $PM_{2.5}$ increased from 0.88 to 0.94. Notably, the spatial correlation for $PM_{2.5}$ and O_3 improved from 0.17 to 0.41 and 0.55 to 0.67, respectively. Additionally, the NMB for NO_2 decreased from −27% to −7%.

However, all participating models persistently underestimated CO concentrations, which is consistent with the KORUS-AQ results. According to the ensemble model results, the NMB value was −55%, even though the model accurately simulated the temporal variation with an R-value of 0.91.

The ensemble model results were found to reproduce the chemical composition of $PM_{2.5}$ well despite significant differences among the models. CMAQ and CMAQ_G models underestimated the NO_3^- concentrations with NMB values of −47% and −56%, respectively, whereas the WRF_GC model significantly overestimated the NO_3^- and NH_4^+ concentrations, with NMB values of 108% and 101%, respectively. These differences may be due to inaccurate meteorological inputs, unexpected precipitation, and low RH, which led to an underestimation of NO_3^- concentrations, and a low level of nighttime PBLH resulted in an overestimation of NO_3^- and NH_4^+ concentrations. During the entire campaign period, all models overestimated EC by a factor of 2–5. This can be attributed to the unusual EC emission levels relating to construction activities near Olympic Park in 2018, which is the reference year of the SIJAQv2 inventory.

Based on a general evaluation of model performance, these intensive campaigns not only help to understand the current air pollution status on the Korean Peninsula, but they also play a major role in guiding CTM performance improvements. The study highlights the importance of accurate meteorological model results, uncertainties in emission inventories, particularly for CO and EC, and the critical role of the temporal allocation of emissions. By addressing these issues, the models would provide more accurate simulations of pollutant concentrations, thereby contributing to more effective air quality management strategies.

CRediT authorship contribution statement

Yesol Cha: Writing – original draft, Methodology, Investigation, Conceptualization. **Jong-Jae Lee:** Writing – original draft, Methodology, Conceptualization. **Chul Han Song:** Writing – review & editing, Methodology, Data curation. **Soontae Kim:** Writing – review & editing, Methodology, Data curation. **Rokjin J. Park:** Writing – review & editing, Methodology, Data curation. **Myong-In Lee:** Writing – review & editing, Methodology, Data curation. **Jung-Hun Woo:** Writing – review & editing, Methodology, Formal analysis, Data curation. **Jae-Ho Choi:** Visualization, Validation, Formal analysis. **Kangho Bae:** Validation, Formal analysis. **Jinhyeok Yu:** Visualization, Software, Formal analysis. **Eunhye Kim:** Validation, Software, Formal analysis. **Hyeonmin Kim:** Validation, Formal analysis, Data curation. **Seung-Hee Lee:** Validation, Software, Data curation. **Jinseok Kim:** Validation, Formal analysis, Data curation. **Lim-Seok Chang:** Writing – review & editing, Funding acquisition, Conceptualization. **Kwon-ho Jeon:** Resources. **Chang-Keun Song:** Writing – review & editing, Supervision, Project administration, Methodology, Funding acquisition, Conceptualization.

Declaration of competing interest

The authors declare that they have no known competing financial interests or personal relationships that could have appeared to influence the work reported in this paper.

Acknowledgements

This work was supported by grants from the Korea Environment Industry & Technology Institute (KEITI) through "Climate Change R&D Project for New Climate Regime" funded by the Korea Ministry of Environment (MOE) [Grant Number 2022003560002] and the National Institute of Environment Research (NIER) funded by the Ministry of Environment (MOE) of the Republic of Korea [Grant Number NIER-2022-04-02-037, NIER-2024-03-02-014, and NIER-2021-03-03-007].

Glossary

CTMs	Chemical transport models
CF	Coarse/fine scheme
CMAQ	Community Multiscale Air Quality Modeling System
CAMx	Comprehensive Air Quality Model with Extensions
EC	Elemental carbon
EBI	Euler Backward Iterative
FNL	Final analysis data
GCAS	GeoCAPE Airborne Simulator
GEMS	Geostationary Environment Monitoring Spectrometer
GFS	Global Forecast System
GOCART	Goddard Chemistry Aerosol Radiation and Transport
GIST	Gwangju Institute of Science and Technology
IOA	Index of Agreement
KORUS-AQ	Korea–United States Air Quality
MB	Mean Bias
MEGAN	Model of Emissions of Gases and Aerosols from Nature
MARGA	Monitor for Aerosols and Gases
MAX-DOAS	Multi-axis Differential Optical Absorption Spectrometer
NCEP	National Center for Environmental Prediction
NIER	National Institute of Environmental Research
NMB	Normalized Mean Bias
OM	Organic matter
PBLH	Planetary boundary layer height
RH	Relative humidity
RMSE	Root Mean Square Error
SOA	Secondary organic aerosols
SMA	Seoul Metropolitan Area
VOCs	Volatile Organic Compounds
WRF	Weather Research and Forecasting
WSM5	WRF Single Moment 5-class

Appendix A. Supplementary data

Supplementary data to this article can be found online at https://doi.org/10.1016/j.atmosenv.2024.120896.

Data availability

Data will be made available on request.

References

Babar, Z.B., Park, J.-H., Kang, J., Lim, H.-J., 2016. Characterization of a smog chamber for studying formation and physicochemical properties of secondary organic aerosol. Aerosol Air Qual. Res. 16 (12), 3102–3113. https://doi.org/10.4209/aaqr.2015.10.0580.

Baklanov, A., Zhang, Y., 2020. Advances in air quality modeling and forecasting. Global Transitions 2, 261–270. https://doi.org/10.1016/j.glt.2020.11.001.

Banta, R.M., Senff, C.J., Alvarez, R.J., Langford, A.O., Parrish, D.D., Trainer, M.K., Darby, L.S., Hardesty, R.M., Lambeth, B., Neuman, J.A., 2011. Dependence of daily peak O3 concentrations near Houston, Texas on environmental factors: wind speed, temperature, and boundary-layer depth. Atmos. Environ. 45 (1), 162–173. https://doi.org/10.1016/j.atmosenv.2010.09.030.

Byun, D., Schere, K.L., 2006. Review of the governing equations, computational algorithms, and other components of the Models-3 Community Multiscale Air Quality (CMAQ) modeling system. Appl. Mech. Rev. 59 (2), 51–77. https://doi.org/10.1115/1.2128636.

Chen, L., Gao, Y., Zhang, M., Fu, J.S., Zhu, J., Liao, H., Li, J., Huang, K., Ge, B., Wang, X., 2019. MICS-Asia III: multi-model comparison and evaluation of aerosol over East Asia. Atmos. Chem. Phys. 19 (18), 11911–11937. https://doi.org/10.5194/acp-19-11911-2019.

Choi, J., Park, R.J., Lee, H.-M., Lee, S., Jo, D.S., Jeong, J.I., Henze, D.K., Woo, J.-H., Ban, S.-J., Lee, M.-D., 2019. Impacts of local vs. trans-boundary emissions from different sectors on PM2. 5 exposure in South Korea during the KORUS-AQ campaign. Atmos. Environ. 203, 196–205. https://doi.org/10.1016/j.atmosenv.2019.02.008.

Choi, W., Ho, C.-H., Heo, J.-W., Kim, K.-Y., Kim, S.-W., Kim, J., 2023. Recent air quality deterioration on weekends in Seoul, South Korea: a focus on external contribution. Asia-Pacific Journal of Atmospheric Sciences 59 (5), 531–543. https://doi.org/10.1007/s13143-022-00287-0.

Crawford, J.H., Ahn, J.-Y., Al-Saadi, J., Chang, L., Emmons, L.K., Kim, J., Lee, G., Park, J.-H., Park, R.J., Woo, J.H., 2021. The Korea–United States air quality (KORUS-AQ) field study. Elem Sci Anth 9 (1), 00163. https://doi.org/10.1525/elementa.2020.00163.

Dominick, D., Juahir, H., Latif, M.T., Zain, S.M., Aris, A.Z., 2012. Spatial assessment of air quality patterns in Malaysia using multivariate analysis. Atmos. Environ. 60, 172–181. https://doi.org/10.1016/j.atmosenv.2012.06.021.

Emmons, L.K., Walters, S., Hess, P.G., Lamarque, J.-F., Pfister, G.G., Fillmore, D., Granier, C., Guenther, A., Kinnison, D., Laepple, T., 2010. Description and evaluation of the model for ozone and related chemical Tracers, version 4 (MOZART-4). Geosci. Model Dev. (GMD) 3 (1), 43–67. https://doi.org/10.5194/gmd-3-43-2010.

ENVIRON, C.U.s.G., 2006. Comprehensive Air Quality model with Extentions, 4.40.

Faisal, A.-A.-., Kafy, A.-A., Abdul Fattah, M., Amir Jahir, D.M., Al Rakib, A., Rahaman, Z. A., Ferdousi, J., Huang, X., 2022. Assessment of temporal shifting of PM2. 5, lockdown effect, and influences of seasonal meteorological factors over the fastest-growing megacity, Dhaka. Spatial Information Research 30 (3), 441–453. https://doi.org/10.1007/s41324-022-00441-w.

Feng, X., Lin, H., Fu, T.-M., Sulprizio, M.P., Zhuang, J., Jacob, D.J., Tian, H., Ma, Y., Zhang, L., Wang, X., 2021. WRF-GC (v2. 0): online two-way coupling of WRF (v3. 9.1. 1) and GEOS-Chem (v12. 7.2) for modeling regional atmospheric chemistry–meteorology interactions. Geosci. Model Dev. (GMD) 14 (6), 3741–3768. https://doi.org/10.5194/gmd-14-3741-2021.

Gaubert, B., Emmons, L.K., Raeder, K., Tilmes, S., Miyazaki, K., Arellano Jr, A.F., Elguindi, N., Granier, C., Tang, W., Barré, J., 2020. Correcting model biases of CO in East Asia: impact on oxidant distributions during KORUS-AQ. Atmos. Chem. Phys. 20 (23), 14617–14647. https://doi.org/10.5194/acp-20-14617-2020.

Grell, G.A., Peckham, S.E., Schmitz, R., McKeen, S.A., Frost, G., Skamarock, W.C., Eder, B., 2005. Fully coupled "online" chemistry within the WRF model. Atmos. Environ. 39 (37), 6957–6975. https://doi.org/10.1016/j.atmosenv.2005.04.027.

Guenther, A., Jiang, X., Heald, C.L., Sakulyanontvittaya, T., Duhl, T.a., Emmons, L., Wang, X., 2012. The Model of Emissions of Gases and Aerosols from Nature version 2.1 (MEGAN2. 1): an extended and updated framework for modeling biogenic emissions. Geosci. Model Dev. (GMD) 5 (6), 1471–1492. https://doi.org/10.5194/gmd-5-1471-2012.

Han, C., Hong, Y.-C., 2020. Decrease in ambient fine particulate matter during COVID-19 crisis and corresponding health benefits in Seoul, Korea. Int. J. Environ. Res. Publ. Health 17 (15), 5279. https://doi.org/10.3390/ijerph17155279.

Hogrefe, C., Liu, P., Pouliot, G., Mathur, R., Roselle, S., Flemming, J., Lin, M., Park, R.J., 2018. Impacts of different characterizations of large-scale background on simulated regional-scale ozone over the continental United States. Atmos. Chem. Phys. 18 (5), 3839–3864. https://doi.org/10.5194/acp-18-3839-2018.

Hong, S.-Y., Dudhia, J., Chen, S.-H., 2004. A revised approach to ice microphysical processes for the bulk parameterization of clouds and precipitation. Mon. Weather Rev. 132 (1), 103–120. https://doi.org/10.1175/1520-0493(2004)132<0103:ARATIM>2.0.CO;2.

Hou, B., Zhuang, G., Zhang, R., Liu, T., Guo, Z., Chen, Y., 2011. The implication of carbonaceous aerosol to the formation of haze: revealed from the characteristics and sources of OC/EC over a mega-city in China. J. Hazard Mater. 190 (1–3), 529–536. https://doi.org/10.1016/j.jhazmat.2011.03.072.

Huang, M., Crawford, J.H., Diskin, G.S., Santanello, J.A., Kumar, S.V., Pusede, S.E., Parrington, M., Carmichael, G.R., 2018. Modeling regional pollution transport events during KORUS-AQ: progress and challenges in improving representation of land-atmosphere feedbacks. J. Geophys. Res. Atmos. 123 (18), 710–756. https://doi.org/10.1029/2018JD028554, 10,732.

Hussein, T., Li, X., Bakri, Z., Alastuey, A., Arar, S., Al-Hunaiti, A., Viana, M., Petäjä, T., 2022. Organic and elemental carbon in the urban background in an eastern mediterranean city. Atmosphere 13 (2), 197. https://doi.org/10.3390/atmos13020197.

Im, U., Christensen, J.H., Geels, C., Hansen, K.M., Brandt, J., Solazzo, E., Alyuz, U., Balzarini, A., Baro, R., Bellasio, R., 2018. Influence of anthropogenic emissions and boundary conditions on multi-model simulations of major air pollutants over Europe and North America in the framework of AQMEII3. Atmos. Chem. Phys. 18 (12), 8929–8952. https://doi.org/10.5194/acp-18-8929-2018.

Jeong, J.I., Park, R.J., 2013. Effects of the meteorological variability on regional air quality in East Asia. Atmos. Environ. 69, 46–55. https://doi.org/10.1016/j.atmosenv.2012.11.061.
Jeong, S., Kim, C., 2021. Bias analysis of WRF-CMAQ simulated PM2. 5 concentrations caused by different PBL parameterizations: application to the haze period of march in 2019 over the Seoul metropolitan area. J. Korean Soc. Atmos. Environ 37, 835–852. https://doi.org/10.5572/KOSAE.2021.37.6.835.
Jordan, C.E., Crawford, J.H., Beyersdorf, A.J., Eck, T.F., Halliday, H.S., Nault, B.A., Chang, L.-S., Park, J., Park, R., Lee, G., 2020. Investigation of factors controlling PM2. 5 variability across the South Korean Peninsula during KORUS-AQ. Elem Sci Anth 8, 28. https://doi.org/10.1525/elementa.424.
Kim, H., Zhang, Q., Heo, J., 2018. Influence of intense secondary aerosol formation and long-range transport on aerosol chemistry and properties in the Seoul Metropolitan Area during spring time: results from KORUS-AQ. Atmos. Chem. Phys. 18 (10), 7149–7168. https://doi.org/10.5194/acp-18-7149-2018.
Kim, S.-U., Kim, K.-Y., 2020. Physical and chemical mechanisms of the daily-to-seasonal variation of PM10 in Korea. Sci. Total Environ. 712, 136429. https://doi.org/10.1016/j.scitotenv.2019.136429.
Kong, L., Tang, X., Zhu, J., Wang, Z., Fu, J.S., Wang, X., Itahashi, S., Yamaji, K., Nagashima, T., Lee, H.-J., 2020. Evaluation and uncertainty investigation of the NO 2, CO and NH 3 modeling over China under the framework of MICS-Asia III. Atmos. Chem. Phys. 20 (1), 181–202. https://doi.org/10.5194/acp-20-181-2020.
Koo, M.-S., Song, K., Kim, J.-E.E., Son, S.-W., Chang, E.-C., Jeong, J.-H., Kim, H., Moon, B.-K., Park, R.J., Yeh, S.-W., 2023. The global/regional integrated model system (GRIMs): an update and seasonal evaluation. Asia-Pacific Journal of Atmospheric Sciences 59 (2), 113–132. https://doi.org/10.1007/s13143-022-00297-y.
Lee, S., Kim, J., Choi, M., Hong, J., Lim, H., Eck, T.F., Holben, B.N., Ahn, J.-Y., Kim, J., Koo, J.-H., 2019. Analysis of long-range transboundary transport (LRTT) effect on Korean aerosol pollution during the KORUS-AQ campaign. Atmos. Environ. 204, 53–67. https://doi.org/10.1016/j.atmosenv.2019.02.020.
Lee, S., Park, R.J., Hong, S.-Y., Koo, M.-S., Jeong, J.I., Yeh, S.-W., Son, S.-W., 2022a. A new chemistry-climate model GRIMs-CCM: model evaluation of interactive chemistry-meteorology simulations. Asia-Pacific Journal of Atmospheric Sciences 58 (5), 647–666. https://doi.org/10.1007/s13143-022-00281-6.
Lee, S., Song, C.H., Han, K.M., Henze, D.K., Lee, K., Yu, J., Woo, J.-H., Jung, J., Choi, Y., Saide, P.E., 2022b. Impacts of uncertainties in emissions on aerosol data assimilation and short-term PM2. 5 predictions over Northeast Asia. Atmos. Environ. 271, 118921. https://doi.org/10.1016/j.atmosenv.2021.118921.
Lennartson, E.M., Wang, J., Gu, J., Castro Garcia, L., Ge, C., Gao, M., Choi, M., Saide, P. E., Carmichael, G.R., Kim, J., 2018. Diurnal variation of aerosol optical depth and PM 2.5 in South Korea: a synthesis from AERONET, satellite (GOCI), KORUS-AQ observation, and the WRF-Chem model. Atmos. Chem. Phys. 18 (20), 15125–15144. https://doi.org/10.5194/acp-18-15125-2018.
Leung, D.M., Shi, H., Zhao, B., Wang, J., Ding, E.M., Gu, Y., Zheng, H., Chen, G., Liou, K. N., Wang, S., 2020. Wintertime particulate matter decrease buffered by unfavorable chemical processes despite emissions reductions in China. Geophys. Res. Lett. 47 (14), e2020GL087721. https://doi.org/10.1029/2020GL087721.
Li, L., Qian, J., Ou, C.-Q., Zhou, Y.-X., Guo, C., Guo, Y., 2014. Spatial and temporal analysis of Air Pollution Index and its timescale-dependent relationship with meteorological factors in Guangzhou, China, 2001–2011. Environ. Pollut. 190, 75–81. https://doi.org/10.1016/j.envpol.2014.03.020.
Lin, H., Feng, X., Fu, T.-M., Tian, H., Ma, Y., Zhang, L., Jacob, D.J., Yantosca, R.M., Sulprizio, M.P., Lundgren, E.W., 2020. WRF-GC (v1. 0): online coupling of WRF (v3. 9.1. 1) and GEOS-Chem (v12. 2.1) for regional atmospheric chemistry modeling–Part 1: description of the one-way model. Geosci. Model Dev. (GMD) 13 (7), 3241–3265. https://doi.org/10.5194/gmd-13-3241-2020.
Liu, X., Ran, L., Lin, W., Xu, X., Ma, Z., Dong, F., He, D., Zhou, L., Shi, Q., Wang, Y., 2022. Measurement report: variations in surface SO 2 and NO x mixing ratios from 2004 to 2016 at a background site in the North China Plain. Atmos. Chem. Phys. 22 (10), 7071–7085. https://doi.org/10.5194/acp-22-7071-2022.
Liu, X., Wang, Y., Wasti, S., Li, W., Soleimanian, E., Flynn, J., Griggs, T., Alvarez, S., Sullivan, J.T., Roots, M., 2023. Evaluating WRF-GC v2. 0 predictions of boundary layer height and vertical ozone profile during the 2021 TRACER-AQ campaign in Houston, Texas. Geosci. Model Dev. (GMD) 16 (18), 5493–5514. https://doi.org/10.5194/gmd-16-5493-2023.
Ma, S., Zhang, X., Gao, C., Tong, D.Q., Xiu, A., Wu, G., Cao, X., Huang, L., Zhao, H., Zhang, S., 2019. Multimodel simulations of a springtime dust storm over northeastern China: implications of an evaluation of four commonly used air quality models (CMAQ v5. 2.1, CAMx v6. 50, CHIMERE v2017r4, and WRF-Chem v3. 9.1). Geosci. Model Dev. (GMD) 12 (11), 4603–4625. https://doi.org/10.5194/gmd-12-4603-2019.
Marécal, V., Peuch, V.-H., Andersson, C., Andersson, S., Arteta, J., Beekmann, M., Benedictow, A., Bergström, R., Bessagnet, B., Cansado, A., 2015. A regional air quality forecasting system over Europe: the MACC-II daily ensemble production. Geosci. Model Dev. (GMD) 8 (9), 2777–2813. https://doi.org/10.5194/gmd-8-2777-2015.
Nault, B.A., Campuzano-Jost, P., Day, D.A., Schroder, J.C., Anderson, B., Beyersdorf, A. J., Blake, D.R., Brune, W.H., Choi, Y., Corr, C.A., 2018. Secondary organic aerosol production from local emissions dominates the organic aerosol budget over Seoul, South Korea, during KORUS-AQ. Atmos. Chem. Phys. 18 (24), 17769–17800. https://doi.org/10.5194/acp-18-17769-2018.
Odum, J.R., Hoffmann, T., Bowman, F., Collins, D., Flagan, R.C., Seinfeld, J.H., 1996. Gas/particle partitioning and secondary organic aerosol yields. Environ. Sci. Technol. 30 (8), 2580–2585. https://doi.org/10.1021/es950943+.
Park, R.J., Oak, Y.J., Emmons, L.K., Kim, C.-H., Pfister, G.G., Carmichael, G.R., Saide, P. E., Cho, S.-Y., Kim, S., Woo, J.-H., 2021. Multi-model intercomparisons of air quality simulations for the KORUS-AQ campaign. Elem Sci Anth 9 (1), 00139. https://doi.org/10.1525/elementa.2021.00139.
Petersen, A.K., Brasseur, G.P., Bouarar, I., Flemming, J., Gauss, M., Jiang, F., Kouznetsov, R., Kranenburg, R., Mijling, B., Peuch, V.-H., 2019. Ensemble forecasts of air quality in eastern China–Part 2: evaluation of the MarcoPolo–Panda prediction system, version 1. Geosci. Model Dev. (GMD) 12 (3), 1241–1266. https://doi.org/10.5194/gmd-12-1241-2019.
Pirovano, G., Balzarini, A., Bessagnet, B., Emery, C., Kallos, G., Meleux, F., Mitsakou, C., Nopmongcol, U., Riva, G., Yarwood, G., 2012. Investigating impacts of chemistry and transport model formulation on model performance at European scale. Atmos. Environ. 53, 93–109. https://doi.org/10.1016/j.atmosenv.2011.12.052.
Qiao, X., Tang, Y., Hu, J., Zhang, S., Li, J., Kota, S.H., Wu, L., Gao, H., Zhang, H., Ying, Q., 2015. Modeling dry and wet deposition of sulfate, nitrate, and ammonium ions in Jiuzhaigou National Nature Reserve, China using a source-oriented CMAQ model: Part I. Base case model results. Sci. Total Environ. 532, 831–839. https://doi.org/10.1016/j.scitotenv.2015.05.108.
Ramsey, N.R., Klein, P.M., Moore III, B., 2014. The impact of meteorological parameters on urban air quality. Atmos. Environ. 86, 58–67. https://doi.org/10.1016/j.atmosenv.2013.12.006.
Schnell, J.L., Naik, V., Horowitz, L.W., Paulot, F., Mao, J., Ginoux, P., Zhao, M., Ram, K., 2018. Exploring the relationship between surface PM 2.5 and meteorology in Northern India. Atmos. Chem. Phys. 18 (14), 10157–10175. https://doi.org/10.5194/acp-18-10157-2018.
Shimadera, H., Hayami, H., Chatani, S., Morino, Y., Mori, Y., Morikawa, T., Yamaji, K., Ohara, T., 2014. Sensitivity analyses of factors influencing CMAQ performance for fine particulate nitrate. J. Air Waste Manag. Assoc. 64 (4), 374–387. https://doi.org/10.1080/10962247.2013.778919.
Skamarock, W.C., Klemp, J.B., 2008. A time-split nonhydrostatic atmospheric model for weather research and forecasting applications. J. Comput. Phys. 227 (7), 3465–3485. https://doi.org/10.1016/j.jcp.2007.01.037.
Sun, J., Qin, M., Xie, X., Fu, W., Qin, Y., Sheng, L., Li, L., Li, J., Sulaymon, I.D., Jiang, L., 2022. Seasonal modeling analysis of nitrate formation pathways in Yangtze River Delta region, China. Atmos. Chem. Phys. 22 (18), 12629–12646. https://doi.org/10.5194/acp-22-12629-2022.
Tang, W., Emmons, L.K., Arellano Jr, A.F., Gaubert, B., Knote, C., Tilmes, S., Buchholz, R. R., Pfister, G.G., Diskin, G.S., Blake, D.R., 2019. Source contributions to carbon monoxide concentrations during KORUS-AQ based on CAM-chem model applications. J. Geophys. Res. Atmos. 124 (5), 2796–2822. https://doi.org/10.1029/2018JD029151.
Tao, H., Xing, J., Zhou, H., Chang, X., Li, G., Chen, L., Li, J., 2018. Impacts of land use and land cover change on regional meteorology and air quality over the Beijing-Tianjin-Hebei region, China. Atmos. Environ. 189, 9–21. https://doi.org/10.1016/j.atmosenv.2018.06.033.
Tiedtke, M., 1989. A comprehensive mass flux scheme for cumulus parameterization in large-scale models. Mon. Weather Rev. 117 (8), 1779–1800. https://doi.org/10.1175/1520-0493(1989)117<1779:ACMFSF>2.0.CO;2.
Travis, K.R., Crawford, J.H., Chen, G., Jordan, C.E., Nault, B.A., Kim, H., Jimenez, J.L., Campuzano-Jost, P., Dibb, J.E., Woo, J.-H., 2022. Limitations in representation of physical processes prevent successful simulation of PM 2.5 during KORUS-AQ. Atmos. Chem. Phys. 22 (12), 7933–7958. https://doi.org/10.5194/acp-22-7933-2022.
Vivanco, M.G., Bessagnet, B., Cuvelier, C., Theobald, M., Tsyro, S., Pirovano, G., Aulinger, A., Bieser, J., Calori, G., Ciarelli, G., 2017. Joint analysis of deposition fluxes and atmospheric concentrations of inorganic nitrogen and sulphur compounds predicted by six chemistry transport models in the frame of the EURODELTAIII project. Atmos. Environ. 151, 152–175. https://doi.org/10.1016/j.atmosenv.2016.11.042.
Wang, Zhou Bin, Z.B., Fu QingYan, F.Q., Zhao QianBiao, Z.Q., Zhang Qi, Z.Q., Chen JianMin, C.J., Yang Xin, Y.X., Duan YuSen, D.Y., Li Juan, L.J., 2016. Intense secondary aerosol formation due to strong atmospheric photochemical reactions in summer: observations at a rural site in eastern Yangtze River Delta of China. https://doi.org/10.1016/j.scitotenv.2016.06.212.
Woo, J.-H., Kim, Y., Kim, H.-K., Choi, K.-C., Eum, J.-H., Lee, J.-B., Lim, J.-H., Kim, J., Seong, M., 2020. Development of the CREATE inventory in support of integrated climate and air quality modeling for Asia. Sustainability 12 (19), 7930. https://doi.org/10.3390/su12197930.
Xie, X., Hu, J., Qin, M., Guo, S., Hu, M., Wang, H., Lou, S., Li, J., Sun, J., Li, X., 2022. Modeling particulate nitrate in China: current findings and future directions. Environ. Int. 166, 107369. https://doi.org/10.1016/j.envint.2022.107369.
Yarwood, G., Jung, J., Whitten, G.Z., Heo, G., Mellberg, J., Estes, M., 2010. Updates to the carbon Bond mechanism for version 6 (CB6). 9th annual CMAS conference. Chapel Hill, NC.
Ye, Z., Li, Q., Ma, S., Zhou, Q., Gu, Y., Su, Y., Chen, Y., Chen, H., Wang, J., Ge, X., 2017. Summertime day-night differences of PM2. 5 components (inorganic ions, OC, EC, WSOC, WSON, HULIS, and PAHs) in Changzhou, China. Atmosphere 8 (10), 189.
Yoo, J.-M., Jeong, M.-J., Kim, D., Stockwell, W.R., Yang, J.-H., Shin, H.-W., Lee, M.-I., Song, C.-K., Lee, S.-D., 2015. Spatiotemporal variations of air pollutants (O 3, NO 2, SO 2, CO, PM 10, and VOCs) with land-use types. Atmos. Chem. Phys. 15 (18), 10857–10885. https://doi.org/10.5194/acp-15-10857-2015.
Zhang, C., Wang, Y., Hamilton, K., 2011. Improved representation of boundary layer clouds over the southeast Pacific in ARW-WRF using a modified Tiedtke cumulus

parameterization scheme. Mon. Weather Rev. 139 (11), 3489–3513. https://doi.org/10.1175/MWR-D-10-05091.1.

Zhang, L., Wang, T., Zhang, Q., Zheng, J., Xu, Z., Lv, M., 2016. Potential sources of nitrous acid (HONO) and their impacts on ozone: a WRF-Chem study in a polluted subtropical region. J. Geophys. Res. Atmos. 121 (7), 3645–3662. https://doi.org/10.1002/2015JD024468.

Zheng, H., Song, S., Sarwar, G., Gen, M., Wang, S., Ding, D., Chang, X., Zhang, S., Xing, J., Sun, Y., 2020. Contribution of particulate nitrate photolysis to heterogeneous sulfate formation for winter haze in China. Environ. Sci. Technol. Lett. 7 (9), 632–638. https://doi.org/10.1021/acs.estlett.0c00368.